Three-Dimensional Modeling of Rigid Pavement

Project Number 7017

Final Report

for

Ohio Department of Transportation

and

Federal Highway Administration

Principal Investigators: D. J. Beegle
S. M. Sargand

The contents of this report reflect the views of the authors, who are responsible for the facts and accuracy of the data presented herein. The contents do not necessarily reflect the official views or policies of the Ohio Department of Transportation or the Federal Highway Administration. This report does not constitute a standard, specification, or regulation.

Ohio University
Civil Engineering Department
September 1995

1. Report No.	2. Government Accession No.	3. Recipient's Catalog No.
ST/SS/95-002		3 1980 00004 5720

4. Title and Subtitle	5. Report Date
THREE DIMENSIONAL MODELING OF RIGID PAVEMENT	February 17, 1995
	6. Performing Organization Code
	8. Performing Organization Report No.
7. Author(s)	10. Work Unit No. (TRAIS)
Shad Sargand, David Beegle	
9. Performing Organization Name and Address	11. Contract or Grant No.
Ohio University Department of Civil Engineering Athens, OH 45701	State Job No. 14537(0)
	13. Type of Report and Period Covered
	Final Report
12. Sponsoring Agency Name and Address	14. Sponsoring Agency Code
Ohio Department of Transportation 25 S. Front St. Columbus, OH 43215	

15. Supplementary Notes

Prepared in cooperation with the U.S. Department of Transportation, Federal Highway Administration

16. Abstract

A finite-element program has been developed to model the response of rigid pavement to both static loads and temperature changes. The program is fully three-dimensional and incorporates not only the common twenty-node brick element but also a thin interface element and a three-node beam element. The interface element is used in the pavement–soil interface and in the joints between slabs. The dowel bars in the joints are modeled by the beam element, which includes flexural and shear deformations. Stresses, strains, and displacements are computed for body forces, traffic loads, and temperature changes individually so that the program can be used to obtain either total stresses for design, or strain changes to compare with experimental data.

The effects of varying the material properties in the pavement, base, subgrade, interfaces, and dowels are investigated to identify those parameters which most influence the solution. Results of various interface thicknesses and dowel diameters also are presented. A further study is conducted to determine the effect of average pavement temperature on the curling stresses and displacements. Finally, results from the program are compared with experimental curling displacements and stresses.

17. Key Words		18. Distribution Statement
Finite-Element Methods Interface Elements Rigid Pavement	Temperature Three-Dimensional Models	No Restrictions. This document is available to the public through the National Technical Information Service, Springfield, Virginia 22161

19. Security Classif. (of this report)	20. Security Classif. (of this page)	21. No. of Pages	22. Price
Unclassified	Unclassified		

Form DOT F 1700.7 (8-72) of completed page authorized

Contents

List of Figures

List of Tables

1
Introduction

A finite-element program was developed for an investigation of the response of rigid pavement to changing environmental conditions and to static loading. The finite-element program has several uncommon features which make it more useful and more flexible than commercially available software for analyzing pavement. Concrete and soil elements are ordinary twenty-node, quadratic, isoparametric hexahedra, but the program uses special thin interface elements to model the behavior of the top layer of soil under the slab. Concrete joints also are represented by interface elements. The interfaces behave as ordinary elements in compression, but in tension they lose stiffness to allow joints to open and slabs to separate from soil.

A three-node isoparametric beam element is used for the joint dowels and ties. The beam element includes both bending and shear deformation to model accurately the deflections of the dowels where they span narrow joints. Longitudinal stiffness is considered for the ties but not for the dowels, which are usually lubricated to prevent development of axial forces.

The program solves nonlinear systems by an iterative secant method. Stresses, strains, and displacements are calculated at each iteration and are used to compute stiffness for the next iteration. The algorithm evaluates stresses resulting from temperature

changes and body forces as well as distributed and concentrated loads. For traffic loads, the displacements, stresses, and strains can be referenced to the results of the first iteration, which includes only stresses produced by the weight of the pavement, for direct comparison with field data. If, on the other hand, thermal stresses are sought, the reference is obtained by running the program with the pavement weight plus the temperature conditions approximately equivalent to those present in the experimental reference state.

2
The Soil and Concrete Elements

Soil and concrete are modeled with a twenty-node, quadratic, isoparametric, hexahedral element [2,3]. This element, with sixty degrees of freedom, provides better accuracy than the usual eight-node linear element, which has 24 degrees of freedom. Although each element has more degrees of freedom, a mesh of twenty-node elements can actually have fewer degrees of freedom than the equivalent mesh of eight-node elements. This is because fewer twenty-node elements are required to give good results. Their quadratic interpolation functions permit them to perform well with high aspect ratios, with curved surfaces, and with coarse meshes. Of course, when a mesh is refined to examine local stresses or displacements in the region of a discontinuity, such as a crack or a dowel bar, the twenty-node elements are far superior to their eight-node counterparts.

Presently, linear elastic material properties are assumed for both soil and concrete, but the program could be amended easily to use nonlinear soil and concrete material models. Similarly, the capability to model crack formation and growth could be added to the program with little difficulty. But for now, it seems that the general behavior of both concrete and soil is represented with acceptable accuracy by linear elastic material models.

2.1 Formulation

The local coordinate system and nodal numbering scheme for the twenty-node element are shown in Figure 2-1. Because the element is isoparametric, the shape functions

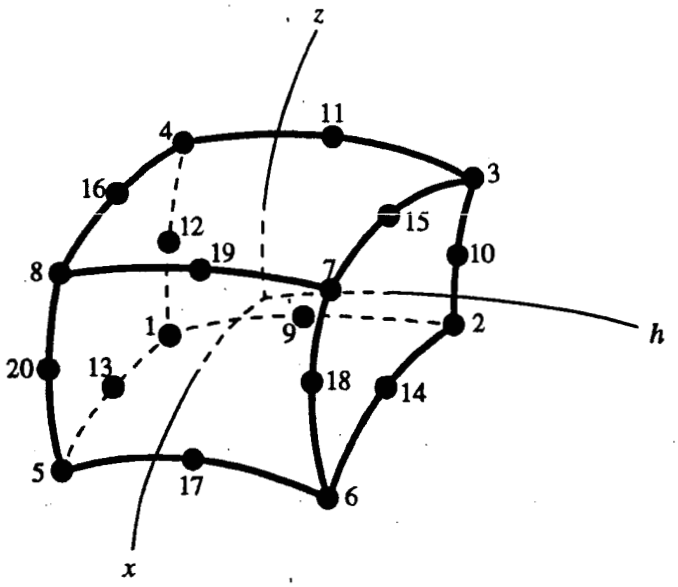

Figure 2-1. Twenty-Node Hexahedral Element.

used for interpolating geometric coordinates are the same as those used for interpolating displacements. The global coordinates corresponding to any point in the local coordinate system are interpolated from the nodal coordinates by

$$x = \sum_{i=1}^{20} N_i x_i \qquad y = \sum_{i=1}^{20} N_i y_i \qquad z = \sum_{i=1}^{20} N_i z_i \tag{2-1}$$

and the displacements are interpolated from their nodal values by

$$u = \sum_{i=1}^{20} N_i u_i \qquad v = \sum_{i=1}^{20} N_i v_i \qquad w = \sum_{i=1}^{20} N_i w_i \tag{2-2}$$

The interpolating polynomials are quadratic functions of the element local coordinates:

$$\begin{aligned}
N_i &= \tfrac{1}{8}(1+\xi\xi_i)(1+\eta\eta_i)(1+\zeta\zeta_i)(\xi\xi_i+\eta\eta_i+\zeta\zeta_i+2) && i = 1,\ 2,\ \ldots,\ 8 \\
N_i &= \tfrac{1}{4}(1-\eta^2)(1+\xi\xi_i)(1+\zeta\zeta_i) && i = 9,\ 11,\ 17,\ 19 \\
N_i &= \tfrac{1}{4}(1-\zeta^2)(1+\xi\xi_i)(1+\eta\eta_i) && i = 10,\ 12,\ 18,\ 20 \\
N_i &= \tfrac{1}{4}(1-\xi^2)(1+\eta\eta_i)(1+\zeta\zeta_i) && i = 13,\ 14,\ 15,\ 16
\end{aligned} \tag{2-3}$$

In these shape functions, ξ_i, η_i, and ζ_i are the coordinates of the nodes in the local coordinate system, as given in Table 2-1.

Table 2-1. Local Coordinates of Nodes for Twenty-Node Element.

i	ξ_i	η_i	ζ_i	i	ξ_i	η_i	ζ_i
1	–1	–1	–1	11	–1	0	1
2	–1	1	–1	12	–1	–1	0
3	–1	1	1	13	0	–1	–1
4	–1	–1	1	14	0	1	–1
5	1	–1	–1	15	0	1	1
6	1	1	–1	16	0	–1	1
7	1	1	1	17	1	0	–1
8	1	–1	1	18	1	1	0
9	–1	0	–1	19	1	0	1
10	–1	1	0	20	1	–1	0

Strains $\boldsymbol{\varepsilon}$ are interpolated within the element from the nodal displacements $\mathbf{q}$ with derivatives of the shape functions.

$$\boldsymbol{\varepsilon} = \mathbf{B}\mathbf{q} = \begin{bmatrix} \mathbf{B}_1 & \mathbf{B}_2 & \cdots & \mathbf{B}_{20} \end{bmatrix} \mathbf{q} \tag{2-4}$$

The derivative submatrices have the form

$$\mathbf{B}_i = \begin{bmatrix} \frac{\partial N_i}{\partial x} & 0 & 0 \\ 0 & \frac{\partial N_i}{\partial y} & 0 \\ 0 & 0 & \frac{\partial N_i}{\partial z} \\ \frac{\partial N_i}{\partial y} & \frac{\partial N_i}{\partial x} & 0 \\ 0 & \frac{\partial N_i}{\partial z} & \frac{\partial N_i}{\partial y} \\ \frac{\partial N_i}{\partial z} & 0 & \frac{\partial N_i}{\partial x} \end{bmatrix} \tag{2-5}$$

These derivatives are taken with respect to the global x–y–z coordinate system, but the interpolation polynomials are functions of the local x–h–z coordinates. The coordinate transformation is accomplished by using the following relationships between the local and global derivatives of the interpolation functions,

$$\begin{aligned} \frac{\partial N_i}{\partial x} &= \frac{\partial N_i}{\partial \xi}\cdot\frac{\partial \xi}{\partial x} & \frac{\partial N_i}{\partial x} &= \frac{\partial N_i}{\partial \eta}\cdot\frac{\partial \eta}{\partial x} & \frac{\partial N_i}{\partial x} &= \frac{\partial N_i}{\partial \zeta}\cdot\frac{\partial \zeta}{\partial x} \\ \frac{\partial N_i}{\partial y} &= \frac{\partial N_i}{\partial \xi}\cdot\frac{\partial \xi}{\partial y} & \frac{\partial N_i}{\partial y} &= \frac{\partial N_i}{\partial \eta}\cdot\frac{\partial \eta}{\partial y} & \frac{\partial N_i}{\partial y} &= \frac{\partial N_i}{\partial \zeta}\cdot\frac{\partial \zeta}{\partial y} \\ \frac{\partial N_i}{\partial z} &= \frac{\partial N_i}{\partial \xi}\cdot\frac{\partial \xi}{\partial z} & \frac{\partial N_i}{\partial z} &= \frac{\partial N_i}{\partial \eta}\cdot\frac{\partial \eta}{\partial z} & \frac{\partial N_i}{\partial z} &= \frac{\partial N_i}{\partial \zeta}\cdot\frac{\partial \zeta}{\partial z} \end{aligned} \tag{2-6}$$

where the derivatives of one coordinate system with respect to the other are obtained from the Jacobian matrix

$$\mathbf{J}=\begin{bmatrix} \dfrac{\partial x}{\partial \xi} & \dfrac{\partial y}{\partial \xi} & \dfrac{\partial z}{\partial \xi} \\ \dfrac{\partial x}{\partial \eta} & \dfrac{\partial y}{\partial \eta} & \dfrac{\partial z}{\partial \eta} \\ \dfrac{\partial x}{\partial \zeta} & \dfrac{\partial y}{\partial \zeta} & \dfrac{\partial z}{\partial \zeta} \end{bmatrix} \tag{2-7}$$

and the terms of the Jacobian matrix are evaluated numerically by

$$\begin{aligned} \frac{\partial x}{\partial \xi}&=\sum_{i=1}^{8}\frac{\partial N_i}{\partial \xi}x_i & \frac{\partial y}{\partial \xi}&=\sum_{i=1}^{8}\frac{\partial N_i}{\partial \xi}y_i & \frac{\partial z}{\partial \xi}&=\sum_{i=1}^{8}\frac{\partial N_i}{\partial \xi}z_i \\ \frac{\partial x}{\partial \eta}&=\sum_{i=1}^{8}\frac{\partial N_i}{\partial \eta}x_i & \frac{\partial y}{\partial \eta}&=\sum_{i=1}^{8}\frac{\partial N_i}{\partial \eta}y_i & \frac{\partial z}{\partial \eta}&=\sum_{i=1}^{8}\frac{\partial N_i}{\partial \eta}z_i \\ \frac{\partial x}{\partial \zeta}&=\sum_{i=1}^{8}\frac{\partial N_i}{\partial \zeta}x_i & \frac{\partial y}{\partial \zeta}&=\sum_{i=1}^{8}\frac{\partial N_i}{\partial \zeta}y_i & \frac{\partial z}{\partial \zeta}&=\sum_{i=1}^{8}\frac{\partial N_i}{\partial \zeta}z_i \end{aligned} \tag{2-8}$$

The six components of the strain vector obtained by Equation 2-4 are three normal strains and three shear strains:

$$\boldsymbol{\varepsilon}=\begin{Bmatrix} \varepsilon_x \\ \varepsilon_y \\ \varepsilon_z \\ \gamma_{xy} \\ \gamma_{yz} \\ \gamma_{zx} \end{Bmatrix}=\begin{Bmatrix} \displaystyle\sum_{i=1}^{20}\frac{\partial N_i}{\partial x}u_i \\ \displaystyle\sum_{i=1}^{20}\frac{\partial N_i}{\partial y}v_i \\ \displaystyle\sum_{i=1}^{20}\frac{\partial N_i}{\partial z}w_i \\ \displaystyle\sum_{i=1}^{20}\frac{\partial N_i}{\partial y}u_i+\sum_{i=1}^{20}\frac{\partial N_i}{\partial x}v_i \\ \displaystyle\sum_{i=1}^{20}\frac{\partial N_i}{\partial z}v_i+\sum_{i=1}^{20}\frac{\partial N_i}{\partial y}w_i \\ \displaystyle\sum_{i=1}^{20}\frac{\partial N_i}{\partial z}u_i+\sum_{i=1}^{20}\frac{\partial N_i}{\partial x}w_i \end{Bmatrix} \tag{2-9}$$

Stresses $\boldsymbol{\sigma}$ are calculated by multiplying the strain vector by the material constitutive matrix **E**.

$$\boldsymbol{\sigma} = \mathbf{E}\boldsymbol{\varepsilon} = \mathbf{EBq} \tag{2-10}$$

The stress components are three normal stresses and three shear stresses

$$\boldsymbol{\sigma} = \{\sigma_x \quad \sigma_y \quad \sigma_z \quad \tau_{xy} \quad \tau_{yz} \quad \tau_{zx}\}^{\mathrm{T}} \tag{2-11}$$

For a linear elastic material, the constitutive matrix **E** is a function of only Young's modulus E and Poisson's ratio n. The linear elastic material matrix used in the program is

$$\mathbf{E} = \frac{E}{(1+\nu)(1-2\nu)} \begin{bmatrix} 1-\nu & \nu & \nu & 0 & 0 & 0 \\ \nu & 1-\nu & \nu & 0 & 0 & 0 \\ \nu & \nu & 1-\nu & 0 & 0 & 0 \\ 0 & 0 & 0 & \frac{1-2\nu}{2} & 0 & 0 \\ 0 & 0 & 0 & 0 & \frac{1-2\nu}{2} & 0 \\ 0 & 0 & 0 & 0 & 0 & \frac{1-2\nu}{2} \end{bmatrix} \tag{2-12}$$

The program computes stresses at the Gauss sampling points used to integrate the stiffness matrix. A $2 \times 2 \times 2$ integration pattern is used by default; other integration grids can be specified, up to $10 \times 10 \times 10$.

The element stiffness matrix **K** relates nodal displacements **q** and nodal forces **p**.

$$\mathbf{Kq} = \mathbf{p} \tag{2-13}$$

The stiffness matrix can be integrated over the volume of the element in global coordinates:

$$\mathbf{K} = \int_V \mathbf{B}^{\mathrm{T}}\mathbf{EB}\, dx\, dy\, dz \tag{2-14}$$

In practice, however, the stiffness matrix is integrated numerically over the local coordinates of the element. The determinant of the Jacobian $|\mathbf{J}|$ is required in the change of variables.

$$\mathbf{K} = \int_{-1}^{1}\int_{-1}^{1}\int_{-1}^{1} \mathbf{B}^{\mathrm{T}}\mathbf{E}\mathbf{B}|\mathbf{J}|\,d\xi\,d\eta\,d\zeta \tag{2-15}$$

2.2 Body Forces

Body forces are applied as equivalent nodal forces, which are computed by numerically integrating the material density over the volume of the element:

$$\mathbf{p}_{\mathrm{b}} = \int_{-1}^{1}\int_{-1}^{1}\int_{-1}^{1} \mathbf{N}^{\mathrm{T}}\mathbf{b}|\mathbf{J}|\,d\xi\,d\eta\,d\zeta \tag{2-16}$$

Here, the interpolating matrix is

$$\mathbf{N} = \left[\begin{array}{ccc:ccc:c:ccc} N_1 & 0 & 0 & N_2 & 0 & 0 & & N_{20} & 0 & 0 \\ 0 & N_1 & 0 & 0 & N_2 & 0 & \cdots & 0 & N_{20} & 0 \\ 0 & 0 & N_1 & 0 & 0 & N_2 & & 0 & 0 & N_{20} \end{array}\right] \tag{2-17}$$

The body force density vector is

$$\mathbf{b} = \begin{Bmatrix} b_x \\ b_y \\ b_z \end{Bmatrix} \tag{2-18}$$

in which b_x, b_y, and b_z are the components of body force density in the x, y, and z directions.

2.3 Thermal Stresses

Temperature changes produce strain, but no stress, in an element which is free to expand and contract, and stress, but no strain, in an element which is completely con-

strained. The displacements and stresses resulting from temperature changes can be produced by equivalent nodal forces, which represent the forces that would be developed in the completely constrained element. Those equivalent nodal forces are

$$\mathbf{p}_T = \int_{-1}^{1}\int_{-1}^{1}\int_{-1}^{1} \mathbf{B}^T \mathbf{E} \boldsymbol{\varepsilon}_{0T} |\mathbf{J}| \, d\xi \, d\eta \, d\zeta \tag{2-19}$$

in which the initial strain vector is

$$\boldsymbol{\varepsilon}_{0T} = \alpha \Delta T \begin{Bmatrix} 1 \\ 1 \\ 1 \\ 0 \\ 0 \\ 0 \end{Bmatrix} \tag{2-20}$$

where a is the coefficient of thermal expansion and ΔT is the temperature change.

2.4 Applications

The twenty-node element is used for both concrete and soil. Its geometry is defined by the x, y, and z coordinates of its nodes, and its behavior is defined by its constitutive model and material properties. In the present version of the program, two material models are available for use with the twenty-node element. The first is the linear elastic material model with two properties, E and n. The linear elastic constitutive matrix was given in Equation 2-12. The second material model for the twenty-node element is the interface model discussed in Chapter 3.

The element gives reasonably accurate results in a coarse mesh, and it is useful at the high aspect ratios encountered in pavement slabs. Moreover, it is very good at modeling curved surfaces, such as the surface between a dowel bar and the surrounding concrete. The output data for the element include displacements and forces at the nodes, and

stresses and strains at the integration points. The standard integration pattern is $2 \times 2 \times 2$, but a separate version of the twenty-node element allows up to $10 \times 10 \times 10$ integration points to be specified in applications in which finer resolution is desired. The standard element with $2 \times 2 \times 2$ integration is provided as a separate element in the program so that its integration routines can be optimized for $2 \times 2 \times 2$ integration.

3
The Interface Element

When the temperature gradient in a slab is such that the slab attempts to curl and to separate from the soil, the soil provides very little resistance against separation. In this situation the ordinary linear elastic material properties must be modified to prevent the formation of tensile stresses perpendicular to the plane of the interface. Also, the friction in the plane of the interface has to be limited so that the shear stress t developed between the slab and the soil is governed by the Mohr–Coulomb criterion, $\tau = c + \sigma_n \tan \phi$, where c is the soil–concrete cohesion, σ_n is the normal compressive stress on the interface, and f is the interface friction angle.

The interface element has been developed to model the behavior at the soil–concrete interface. The interface element is an ordinary twenty-node hexahedral element, but its material properties are manipulated to control the stresses in the interface. The thickness of the interface element is relatively small compared to its other two dimensions, as shown in Figure 3-1. It must be thin enough that it models only the actual interface layer of the soil, but thick enough that its aspect ratio does not cause numerical problems. The thickness of the interface layer under a slab is typically one to three inches. In tests, one-inch and three-inch elements have given nearly identical results.

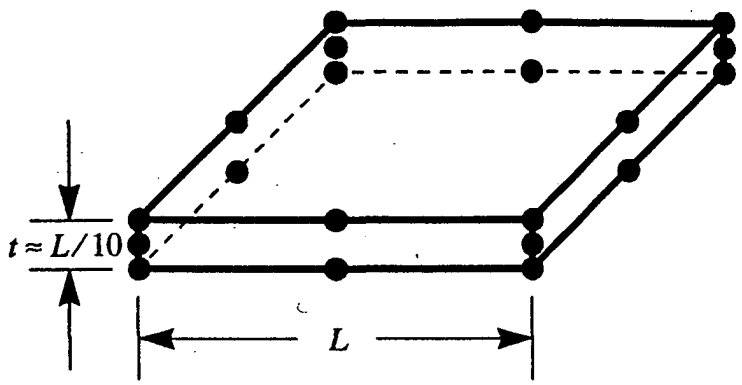

Figure 3-1. Twenty-Node Thin Interface Element.

3.1 Formulation

The basic formulation of the interface element is identical to that presented in Chapter 2 for the twenty-node hexahedral element. The only difference is in the material matrix **E**. The interface material properties are determined in each iteration of the finite-element solution according to the stresses from the previous iteration. The material constitutive matrix is a modified form of Equation 2-12,

$$\mathbf{E} = \begin{bmatrix} \frac{E_{min}(1-\nu)}{(1+\nu)(1-2\nu)} & \frac{E_n\nu}{(1+\nu)(1-2\nu)} & \frac{E_n\nu}{(1+\nu)(1-2\nu)} & 0 & 0 & 0 \\ \frac{E_n\nu}{(1+\nu)(1-2\nu)} & \frac{E_{min}(1-\nu)}{(1+\nu)(1-2\nu)} & \frac{E_n\nu}{(1+\nu)(1-2\nu)} & 0 & 0 & 0 \\ \frac{E_n\nu}{(1+\nu)(1-2\nu)} & \frac{E_n\nu}{(1+\nu)(1-2\nu)} & \frac{E_n(1-\nu)}{(1+\nu)(1-2\nu)} & 0 & 0 & 0 \\ 0 & 0 & 0 & G_{min} & 0 & 0 \\ 0 & 0 & 0 & 0 & G_n & 0 \\ 0 & 0 & 0 & 0 & 0 & G_n \end{bmatrix} \quad (3\text{-}1)$$

in which E_{min} and G_{min} are small numbers just large enough to avoid numerical difficulties and E_n and G_n are determined according to the following algorithm: If the normal stress σ_n is positive, indicating that the interface is in tension, the normal modulus and the two in-plane shear moduli are assigned small values, $E_n = E_{min}$ and $G_n = G_{min}$, so that the tension and shear in the interface will be very small. Otherwise, if σ_n is negative, the normal modulus is equal to the linear elastic Young's modulus, and the in-plane shear moduli are reduced, if necessary, so that the maximum in-plane shear stress will not exceed $\tau = c + \sigma_n \tan\phi$, as follows:

$$E_n = E$$
$$G_n = \frac{(c + \sigma_n \tan\phi)}{\sqrt{\gamma_{13}^2 + \gamma_{23}^2}}, \quad G_{min} \le G_n \le G \tag{3-2}$$

Finally, the new E_n and G_n are compared to the E_n and G_n from the preceding iteration to be certain that the moduli are not increasing. If one of the moduli is found to have a value greater than that of the preceding iteration, it is assigned the value that it had in the preceding iteration. In this way, the interface is not permitted to become stronger after it has weakened.

Figure 3-2 shows the stress–strain curve for the normal direction for the interface element. The cohesion c is usually set to zero for both concrete–concrete and soil–concrete interfaces. Then, the normal modulus becomes $E_n = E_{min}$ immediately when σ_n becomes positive. Of course, the interface behaves as an ordinary linear elastic material in compression. Figure 3-3 shows the in-plane shear stress–strain curves. Figure 3-3(a) shows that the in-plane shear modulus is $G_n = G_{min}$ when the interface is in tension. In compression, the shear stress–strain curve is similar to that for a linear elastic material except that it flattens at $\pm(c + \sigma_n \tan\phi)$, as in Figure 3-3($b$).

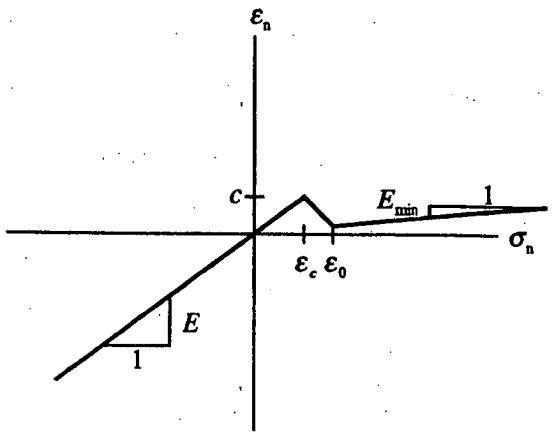

Figure 3-2. Normal Stress–Strain Curve for Interface.

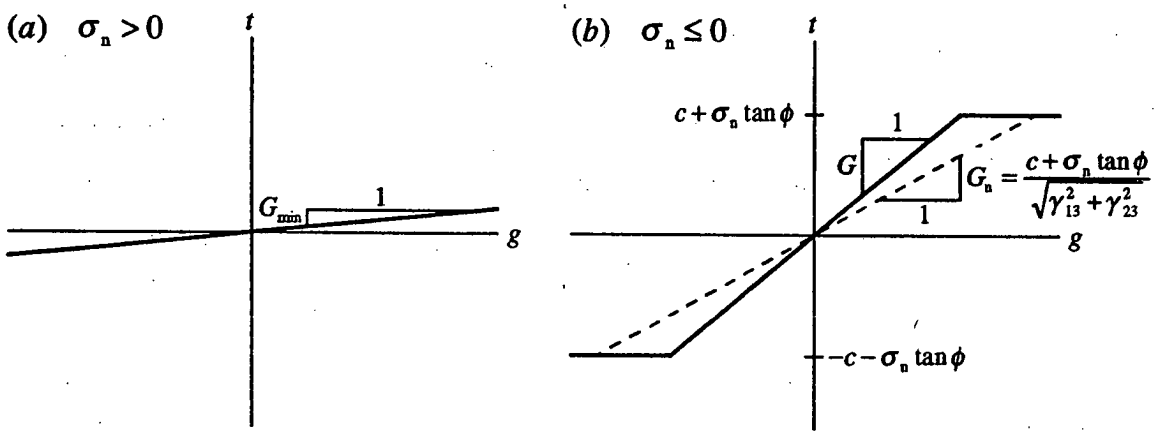

Figure 3-3. In-Plane Shear Stress–Strain Curves for Interface.

The material properties are computed individually at each integration point in the interface element. For even greater accuracy, more integration points can be used in the plane of the interface. The program defaults to a $2 \times 2 \times 2$ Gauss integration, but Gauss or Newton–Cotes integration can be specified for up to $10 \times 10 \times 10$ points. It is usually desirable to use just two points in the direction normal to the interface because the inter-

face is relatively thin and therefore has approximately constant stresses throughout its thickness. Moreover, using more points requires more computation time. The use of only one integration point in the normal direction—or in any direction—is to be discouraged: Although the interface element is thin, it uses the same quadratic interpolation functions in the normal direction as in the other two directions, so it does require at least two-point Gauss quadrature to give accurate results.

3.2 Applications

The interface element is used between the pavement slabs and the underlying soil, and in the joints between adjacent slabs. The input and output data for the interface element itself are the same as discussed in Section 2.4 for the soil and concrete elements, but the material properties for the interface are somewhat more complex. In addition to the material properties required for a linear elastic material, the interface material has four other properties, the cohesion c, the strain ε_0 at which tensile stress becomes zero, the minimum modulus E_{min}, and the in-plane friction angle f.

For the interface under a slab, the interface material is given the properties of the soil immediately below the slab. The cohesion c is usually set to zero, and in that case the strain ε_0 is irrelevant. The minimum modulus E_{min} is chosen to be very small compared to Young's modulus E, but not small enough to cause an ill-conditioned stiffness matrix. In the concrete–concrete joints, the interface materials are given zero cohesion and a minimum modulus E_{min} which is about the same as the E_{min} under the slab. The other properties, particularly E and f, must be chosen carefully to produce realistic results. Reasonable values for E and f can be obtained in the laboratory.

Another consideration for an interface element is its normal direction. The program presently allows three choices of the interface normal direction—x, y, and z. Each direction has its own corresponding material routines in the program. The program was

arranged this way so that no coordinate transformations are required to rotate the material matrix into the global coordinate system. New material routines could be added easily to permit the interface normal direction to be specified by three direction cosines. However, stresses, strains, and the material matrices then would have to be rotated from the element coordinate system to the global coordinate system. Each rotation requires two matrix multiplications, so the material routines would not execute as quickly as the ones presently available in the program. Furthermore, the interface directions presently available are sufficient for modeling pavement.

4
The Beam Element

It is common in finite-element analysis of pavements to neglect the effects of the dowels in the joints between slabs, and of the ties connecting the slab to the shoulder and to the adjacent lane. However, the dowels and ties do have a significant influence on the behavior of the pavement both when the temperature varies throughout the depth of the slab and when the slab is loaded near the joint. While the dowels usually carry no longitudinal forces, they can carry large bending and shear forces across the joints. The ties, on the other hand, are of a smaller diameter and carry little bending or shear, but they develop large longitudinal forces.

The dowels and ties are modeled with three-node isoparametric beam elements which include both flexural and shear deformation. The contribution of shear to the deformation of the dowels is important because the dowels are essentially deep beams: They carry relatively large shear forces across short spans in the joints.

4.1 Formulation

The three-node isoparametric beam element, shown in Figure 4-1, is based on an element developed by Hinton and Owen [1]. This element formulation includes shear, as well as flexural, deformation. Ordinary beam elements are formulated by ass g that

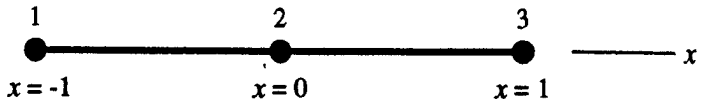

Figure 4-1. Three-Node Beam Element.

plane sections normal to the neutral axis remain plane and normal in bending, as in Figure 4-2. When shear becomes important, that assumption loses validity. The originally plane

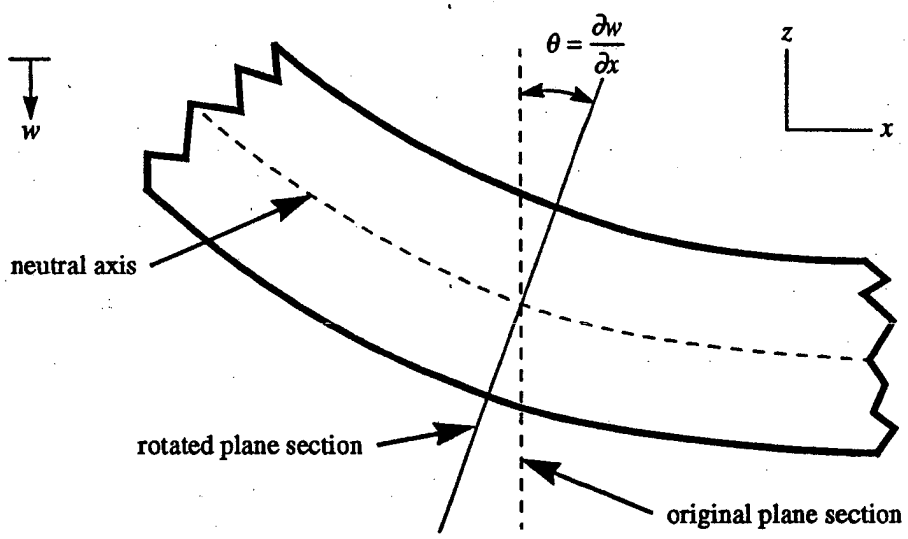

Figure 4-2. Rotation of Plane Section in Simple Beam Theory.

and normal sections deform and rotate as shown in Figure 4-3. The rotation of a normal plane section of the usual thin beam is assumed to be

$$\theta = \frac{\partial w}{\partial x} \tag{4-1}$$

but for a thick beam in which shear deformation is considered, the rotation is approximated by

$$\theta = \frac{\partial w}{\partial x} + \phi \tag{4-2}$$

in which f is an extra shear rotation. The potential energy function of such a one-dimensional beam in flexure is

$$\pi = \tfrac{1}{2}\int EI\left(\frac{\partial \theta}{\partial x}\right)^2 dx + \int S\phi^2 dx \tag{4-3}$$

where EI = bending stiffness,

$\frac{\partial \theta}{\partial x}$ = apparent curvature,

$S = \frac{GA}{\alpha}$ = shear stiffness,

α = a warping factor, and

ϕ = approximate shear rotation.

The beam element has three equally spaced nodes. If axial displacements are ignored, as they are for the dowels, the element has twelve degrees of freedom, two translations and two rotations at each node. In this case the displacement vector is

$$\mathbf{q} = \left\{v_1 \quad \theta_{z1} \quad w_1 \quad \theta_{y1} \;\vdots\; v_2 \quad \theta_{z2} \quad w_2 \quad \theta_{y2} \;\vdots\; v_3 \quad \theta_{z3} \quad w_3 \quad \theta_{y3}\right\}^{\mathrm{T}} \tag{4-4}$$

and the interpolation functions are

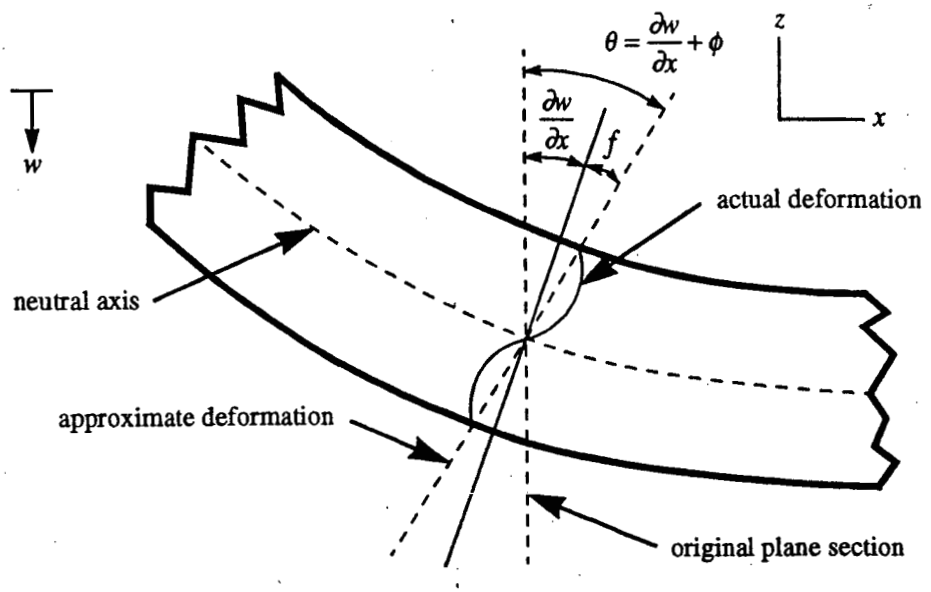

Figure 4-3. Deformation of Plane Section of Beam in Flexure and Shear.

$$N_1 = -\tfrac{1}{2}\xi(1-\xi)$$
$$N_2 = (1-\xi)(1+\xi) \qquad (4\text{-}5)$$
$$N_3 = \tfrac{1}{2}\xi(1+\xi)$$

The displacements and rotations are interpolated as

$$v(\xi) = \sum_{i=1}^{3} N_i v_i \qquad w(\xi) = \sum_{i=1}^{3} N_i w_i$$
$$\theta_z(\xi) = \sum_{i=1}^{3} N_i \theta_{zi} \qquad \theta_y(\xi) = \sum_{i=1}^{3} N_i \theta_{yi} \qquad (4\text{-}6)$$

For this beam formulation, the strains are defined as

$$\boldsymbol{\varepsilon} = \begin{Bmatrix} \dfrac{\partial \theta_z}{\partial x} \\ \phi_z \\ \dfrac{\partial \theta_y}{\partial x} \\ \phi_y \end{Bmatrix} = \mathbf{B}\mathbf{q} = \begin{bmatrix} \mathbf{B}_1 & \mathbf{B}_2 & \mathbf{B}_3 \end{bmatrix} \mathbf{q} \tag{4-7}$$

where

$$\mathbf{B}_i = \begin{bmatrix} 0 & \dfrac{\partial N_i}{\partial x} & 0 & 0 \\ -\dfrac{\partial N_i}{\partial x} & N_i & 0 & 0 \\ 0 & 0 & 0 & \dfrac{\partial N_i}{\partial x} \\ 0 & 0 & -\dfrac{\partial N_i}{\partial x} & N_i \end{bmatrix} \tag{4-8}$$

The derivatives in **B** are taken with respect to the global coordinate x. They are related to the local coordinate x by

$$\frac{\partial N_i}{\partial x} = \frac{\partial N_i}{\partial \xi} \cdot \frac{\partial \xi}{\partial x} = \frac{\partial N_i}{\partial \xi} \cdot \frac{2}{L} \tag{4-9}$$

if the nodes are evenly spaced. The shear force and bending moment are treated as stresses:

$$\begin{Bmatrix} M_z \\ Q_y \\ My \\ Q_z \end{Bmatrix} = \begin{bmatrix} EI_z & 0 & 0 & 0 \\ 0 & S_y & 0 & 0 \\ 0 & 0 & EI_y & 0 \\ 0 & 0 & 0 & S_z \end{bmatrix} \begin{Bmatrix} \frac{\partial \theta_z}{\partial x} \\ \phi_z \\ \frac{\partial \theta_y}{\partial x} \\ \phi_y \end{Bmatrix} \tag{4-10}$$

or

$$\boldsymbol{\sigma} = \mathbf{C}\boldsymbol{\varepsilon} \tag{4-11}$$

The stiffness matrix is calculated in the usual way,

$$\mathbf{K} = \int_L \mathbf{B}^T \mathbf{C} \mathbf{B}\, dx \tag{4-12}$$

which, in local coordinates, becomes

$$\mathbf{K} = \int_{-1}^{1} \mathbf{B}^T \mathbf{C} \mathbf{B} \frac{L}{2} d\xi \tag{4-13}$$

The stiffness matrix is integrated numerically even though for this element it could be evaluated explicitly.

4.2 Tie Element

For the ties, an axial translation is added to each node. The displacement vector for the tie element is

$$\mathbf{q} = \{ v_1 \quad \theta_{z1} \quad w_1 \quad \theta_{y1} \quad u_1 \mid v_2 \quad \theta_{z2} \quad w_2 \quad \theta_{y2} \quad u_2 \mid v_3 \quad \theta_{z3} \quad w_3 \quad \theta_{y3} \quad u_3 \}^T \tag{4-14}$$

and its stress-strain relationship is

$$\begin{Bmatrix} M_z \\ Q_y \\ M_z \\ Q_y \\ \sigma_x \end{Bmatrix} = \begin{bmatrix} EI_z & 0 & 0 & 0 & 0 \\ 0 & S_y & 0 & 0 & 0 \\ 0 & 0 & EI_y & 0 & 0 \\ 0 & 0 & 0 & S_z & 0 \\ 0 & 0 & 0 & 0 & E \end{bmatrix} \begin{Bmatrix} \frac{\partial \theta_z}{\partial x} \\ \phi_z \\ \frac{\partial \theta_y}{\partial x} \\ \phi_y \\ \varepsilon_x \end{Bmatrix} \tag{4-15}$$

The strains for this element are given by Equation 4-7 with the **B** matrix extended to include the axial degrees of freedom:

$$\mathbf{B}_i = \begin{bmatrix} 0 & \frac{\partial N_i}{\partial x} & 0 & 0 & 0 \\ -\frac{\partial N_i}{\partial x} & N_i & 0 & 0 & 0 \\ 0 & 0 & 0 & \frac{\partial N_i}{\partial x} & 0 \\ 0 & 0 & -\frac{\partial N_i}{\partial x} & N_i & 0 \\ 0 & 0 & 0 & 0 & \frac{\partial N_i}{\partial x} \end{bmatrix} \tag{4-16}$$

4.3 Applications

Two different versions of the beam element are available in the program. First is a dowel element with no longitudinal degrees of freedom. Consequently, the dowel element does not resist opening of the joints. The second beam element is a tie element. It does have a longitudinal stiffness to keep adjoining slabs tied together. For both of these beam elements, the input data include the coordinates of the nodes, the orientation of the longitudinal axis, and the material properties. The longitudinal axis must be oriented along either the *x*, *y*, or *z* direction, and the principal axes of inertia of the beam cross-section must be aligned with the other two axes. Execution speed is increased as a result of these

requirements since no coordinate transformations are necessary. Furthermore, these restrictions on the orientation of the beam elements are really not a limitation for pavement analysis. If arbitrarily aligned beam elements were needed, they could be added to the program easily.

The material properties to be specified for a beam are given in Table 4-1. The first and second axes for bending are identified in Table 4-2.

Table 4-1. Material Properties for Beam Elements.

Property	Description
E	Young's modulus
n	Poisson's ratio
A	cross-sectional area
I_1	moment of inertia about first axis
I_2	moment of inertia about second axis
α_1	warping factor for bending about first axis
α_2	warping factor for bending about second axis

Table 4-2. First and Second Axes for Bending of Beam Element.

Longitudinal Axis	Bending Axis 1	Bending Axis 2
x	y	z
y	z	x
z	x	y

5
The Finite-Element Procedure

The finite-element program is designed to solve problems with nonlinear material response. The interface elements are currently the only ones using nonlinear material models, but the other elements could be given nonlinear characteristics by a very simple addition to the program. Solution of the nonlinear problems is accomplished by using an iterative secant method, in which the stresses and strains at each iteration are used to determine the stiffnesses of the nonlinear materials for the next iteration.

The output of the finite-element program includes stresses, strains, and displacements in the pavement slab and the soil. For pavement analysis or design, the total stresses and strains reported by the program are the desired quantities, but for comparison with experimental data, some reference data corresponding to the residual stresses present at the experimental zero state must be subtracted from the output quantities. Obtaining the reference stresses and displacements requires the solution of another entire problem corresponding to the experimental reference state.

5.1 Solution Algorithm

The first iteration of the program includes only body forces. All materials are assumed to be under no stress for the purpose of calculating material properties, and those

properties are assumed to be constant. The stresses, strains, and displacements for the first iteration are saved to disk for later reference. The second iteration applies all forces—body, thermal, and traffic—and uses the stresses and strains from the first iteration to calculate the material properties. Displacements, stresses, and strains are computed.

The third iteration again applies all of the loads. Stresses and strains from the second iteration are used to find material properties. Again, Displacements, stresses, and strains are computed. This process is repeated until the change in the displacement vector, as defined below, becomes less than a specified tolerance.

$$\text{change} = \frac{\sum_i (q_i^k - q_i^{k-1})^2}{\sum_i (q_i^k)^2} \tag{5-1}$$

When the iterations have converged to within the specified tolerance, the program writes the final displacements, stresses, and strains to disk.

5.2 Reference Data

If the output results are to be compared with experimental data, it is necessary to run a separate problem to get the stresses, strains, and displacements of the reference state. The reference problem includes body forces and temperatures corresponding to the experimental zero condition. The basic assumption of this method is that there exists some temperature at which stresses and displacements are zero. The problem that is solved is a temperature change from that rest temperature to the temperature of interest. Then the reference problem is a temperature change from the rest temperature to the temperature at which the experimental data was zeroed.

6
Verification of the Program

The finite-element program was used to solve several highway pavement problems. Each problem consisted of a concrete pavement slab, a base layer, and a subgrade layer. A layer of interface elements separated the concrete from the base to model concrete–soil separation and friction. The slab was connected by dowels to other slabs on two sides, and by ties to another slab on one side. Figure 6-1 shows a typical slab with dowelled end joints and a tied side. In some problems, a tied shoulder was added, as in Figure 6-2. In both dowelled and tied slab–slab joints, interface elements were used between slabs to simulate load transfer across the joint and to permit compression but to prevent tension.

6.1 Finite-Element Mesh

Figure 6-3 shows a typical finite-element mesh cross section in the x–z plane. Five layers of elements can be seen: two layers of concrete elements, one layer of interface elements, one layer of base elements, and two layers of subgrade elements. Figure 6-4 shows the y–z plane cross section, and Figure 6-5 shows the top view of the x–y plane. Note that for most of the problems that were solved, the concrete shoulder was not tied to the main slab.

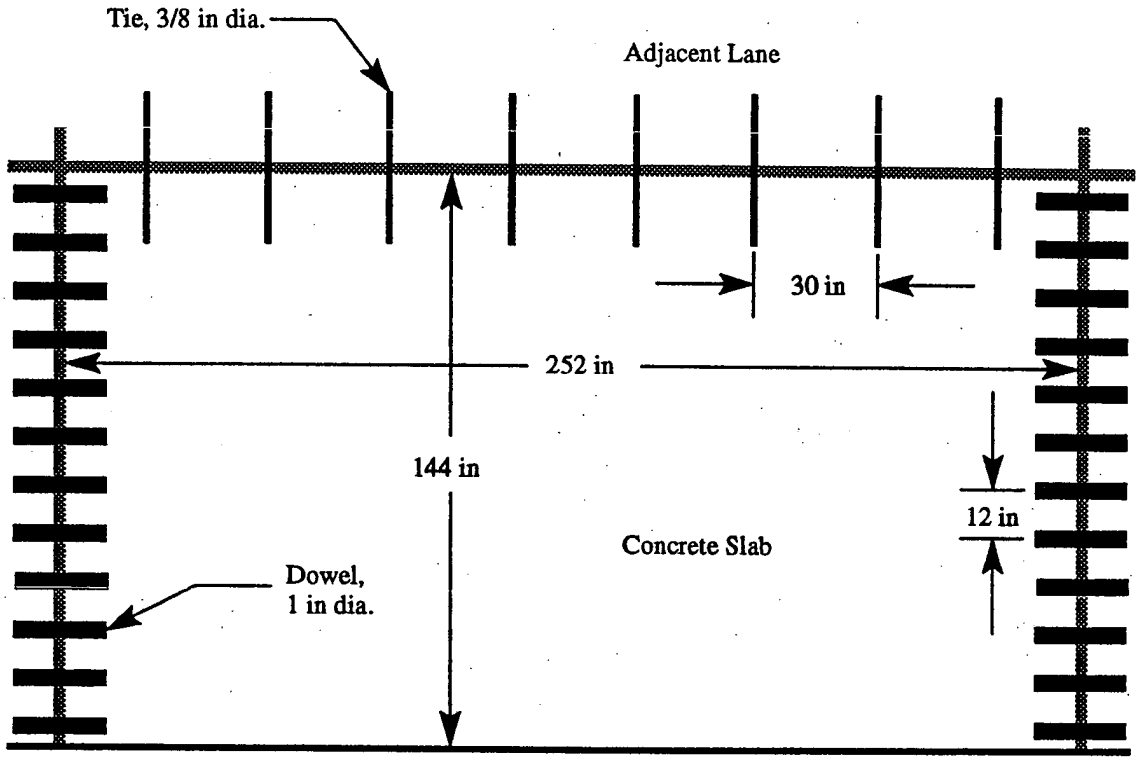

Figure 6-1. A slab with dowelled end joints, one tied edge, and no shoulder.

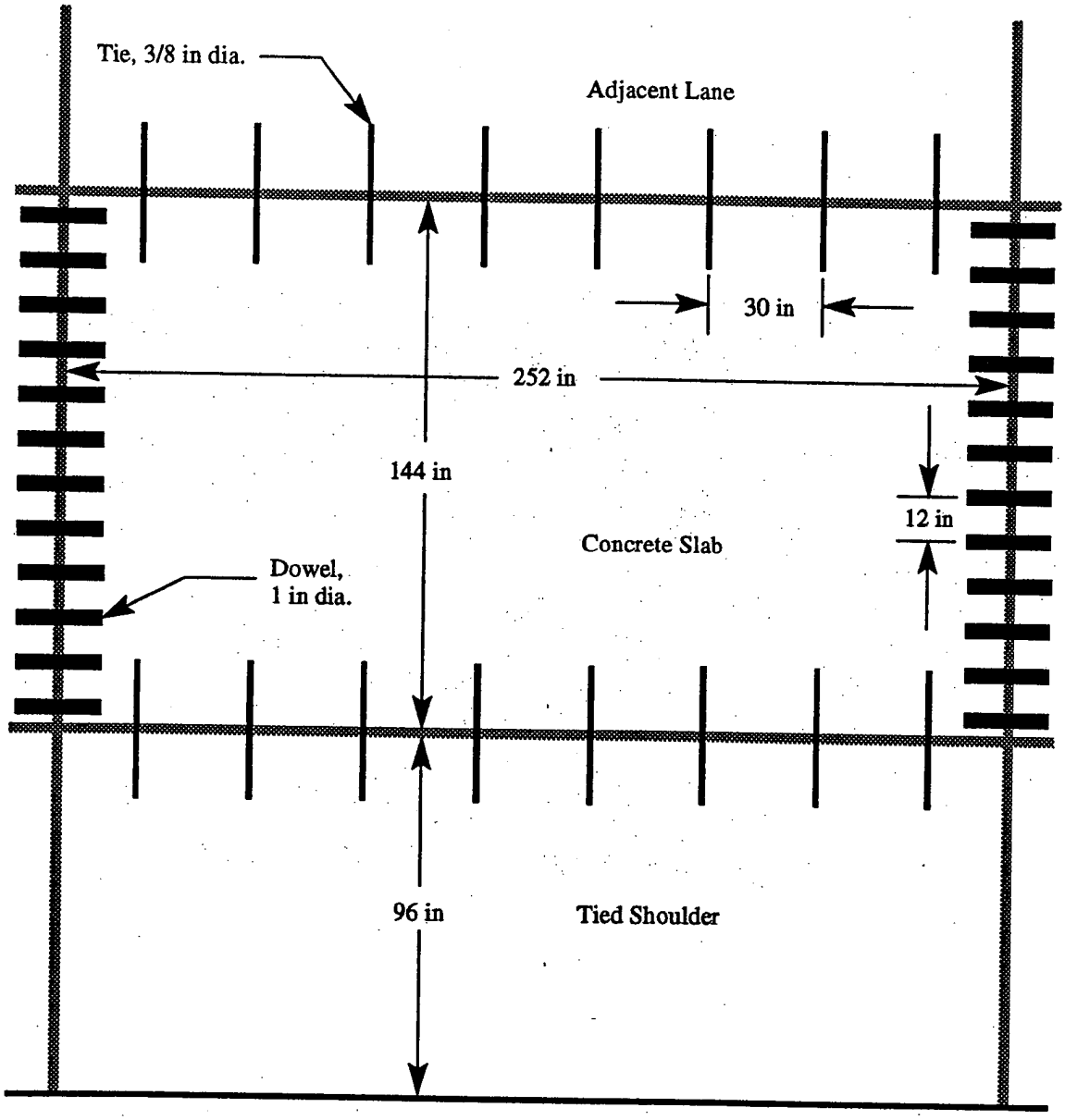

Figure 6-2. A slab with dowelled end joints and tied edges.

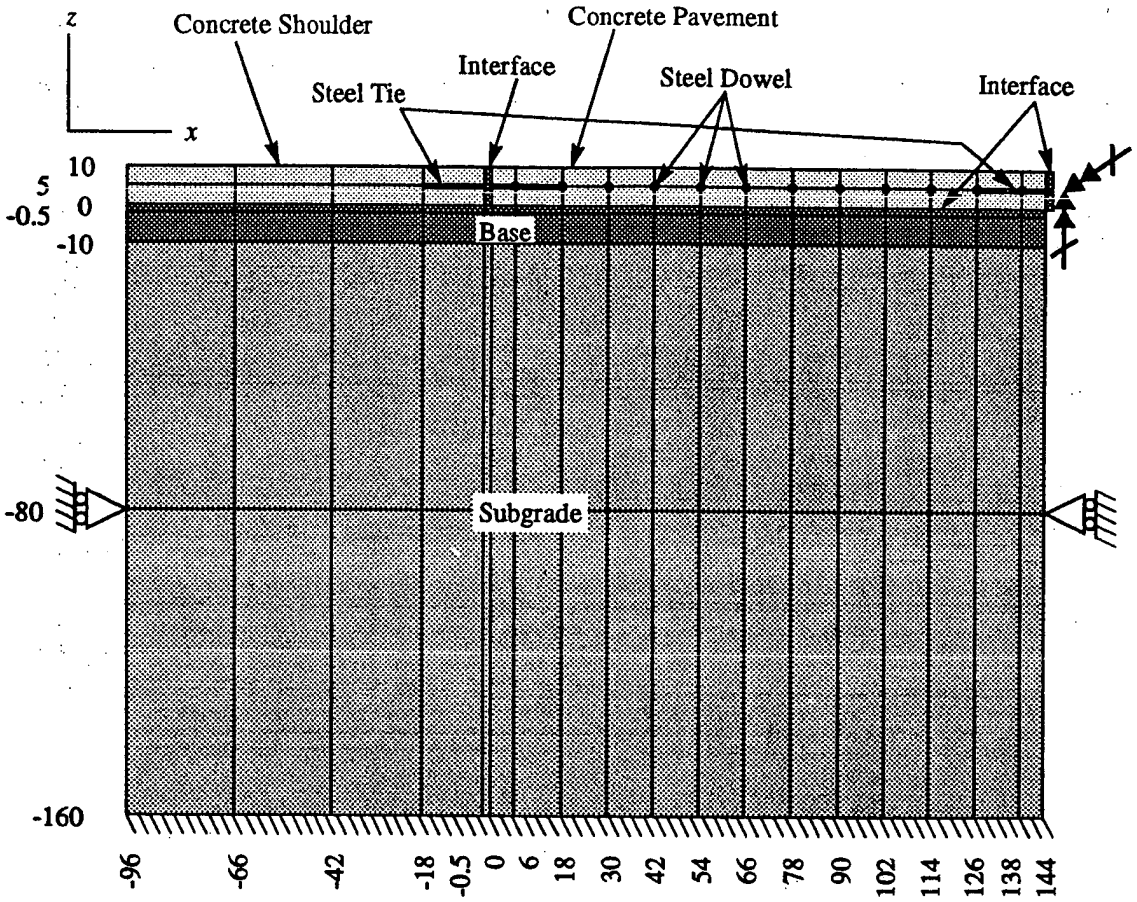

Figure 6-3. Mesh cross-section in x–z plane.

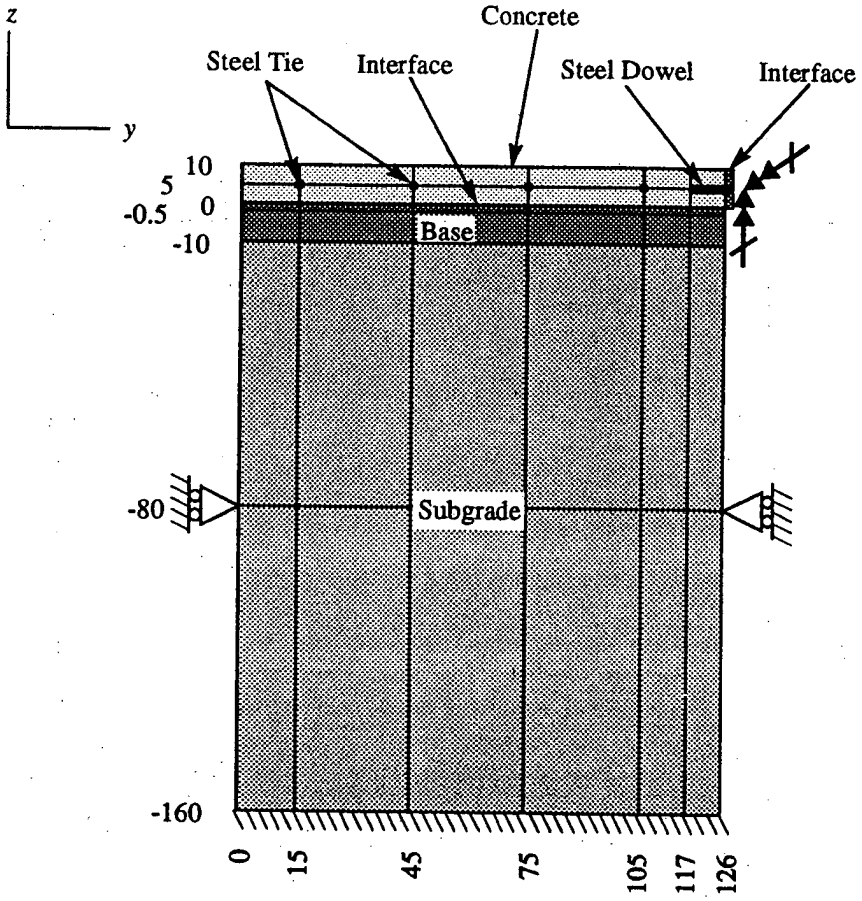

Figure 6-4. Mesh cross-section in y–z plane.

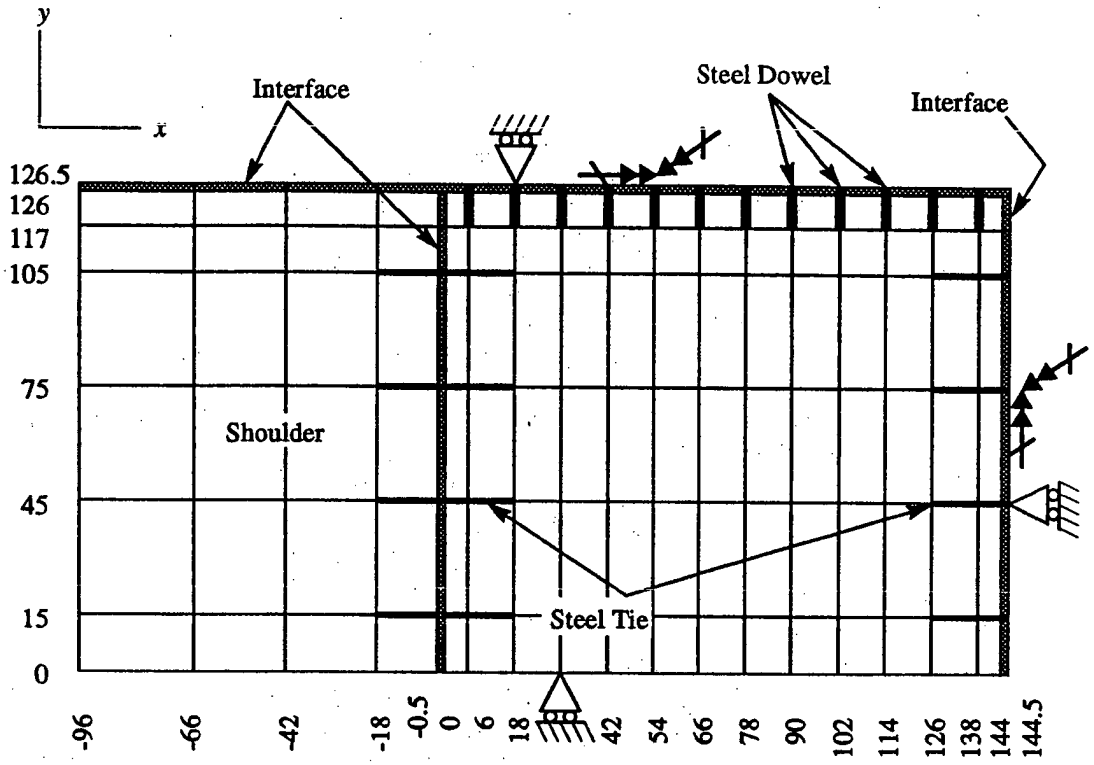

Figure 6-5. Mesh cross-section in *x*–*y* plane.

6.2 Material Properties

The sample problems were run with various values of the material parameters and for both positive and negative temperature gradients. Table 6-1 gives the material parameters used for the sample problems. The positive-gradient temperatures are shown in Table 6-2, and the temperatures for the negative gradient are given in Table 6-3. The most important of the material properties are discussed in the following sections.

6.2.1 Concrete. The elastic modulus of the concrete pavement layer has a predictable effect on the vertical displacements in the case of a positive temperature gradient; a larger modulus generally produces larger displacements in both the positive and negative directions, as shown in Figure 6-6. For the negative temperature gradient, the effect of the concrete modulus is less pronounced and, as can be seen in Figure 6-7, less predictable.

6.2.2 Subgrade. The elastic modulus of the subgrade controls the sinking of the pavement into the soil when part of the concrete layer loses contact with the base. For the positive temperature gradient, a weaker soil allows the edges of the slab to sink deeper and the center to rise higher, as Figure 6-8 shows. Figure 6-9 shows that with a negative temperature gradient, the weaker soil permits the slab to sink more and results in an increased contact area between the slab and the base.

6.2.3 Concrete–Concrete Interface. The modulus of the concrete–concrete interface governs the normal stiffness of the thin interface elements under compression. It also determines the shear stiffness if the shear stress is below the allowable maximum. Figure 6-10 shows the results of reducing the concrete–concrete interface stiffness by a factor of ten under a positive temperature gradient. Figure 6-11 shows the corresponding data for a negative temperature gradient.

Table 6-1. Material properties used in the test problems. When more than one value is listed, the value used for most problems is given in bold type.

Material	Parameter	Description	Value(s)	Units
concrete	E_c	Elastic modulus	3000, **4000**, 5000	ksi
	ν_c	Poisson ratio	0.25	1
	γ_c	Weight density	0.085	lb/in^3
	α_c	Thermal strain coefficient	5.5	me/°F
base	E_b	Elastic modulus	15, **30**, 50	ksi
	ν_b	Poisson ratio	0.3	1
subgrade	E_s	Elastic modulus	5, **10**, 15	ksi
	ν_s	Poisson ratio	0.3	1
dowel	E_d	Elastic modulus	30000	ksi
	ν_d	Poisson ratio	0.3	1
	d_d	Diameter	0.5, **1.0**, 1.5	in
tie	E_t	Elastic modulus	30000	ksi
	ν_t	Poisson ratio	0.3	1
	d_t	Diameter	**3/8**, 5/8	in
concrete–concrete interface	$E_{c\text{-}c}$	Elastic modulus	400, **4000**	ksi
	$\nu_{c\text{-}c}$	Poisson ratio	0.15, **0.2**, 0.3	1
	$E_{c\text{-}c\,min}$	Minimum elastic modulus	10.0	psi
	$\tan\phi_{c\text{-}c}$	Tangent of friction angle	**1.0**, 10.0	1
	$t_{c\text{-}c}$	Thickness	0.1, **0.5**, 1.0	in
concrete–soil interface	$E_{c\text{-}s}$	Elastic modulus	50, **500**, 1000	ksi
	$\nu_{c\text{-}s}$	Poisson ratio	0.15, **0.3**, 0.4	1
	$E_{c\text{-}s\,min}$	Minimum elastic modulus	10.0	psi
	$\tan\phi_{c\text{-}s}$	Tangent of friction angle	**1.0**, 10.0	1
	$t_{c\text{-}s}$	Thickness	**0.5**, 1.0, 2.0	in

Table 6-2. Temperature profile of pavement with positive gradient (warmer top).

Depth, in	Temperature change, °F
0.0	–10.4
2.5	–15.4
5.0	–19.1
7.5	–20.9
10.0	–22.1

Table 6-3. Temperature profile of pavement with negative gradient (cooler top).

Depth, in	Temperature change, °F
0.0	–31.3
2.5	–27.6
5.0	–25.8
7.5	–23.9
10.0	–22.9

The small effect of the friction angle of the interface can be seen in Figure 6-12. The friction angle makes no discernible difference for the positive temperature gradient.

6.2.4 Concrete–Soil Interface. Changes in the friction angle of the concrete–soil interface resulted in relatively minor changes in the displacements of the concrete layer. Figure 6-13 shows the positive-gradient case, and Figure 6-14 shows the negative-gradient case.

For the positive temperature gradient, a thicker concrete–soil interface gave a smaller contact area; see Figure 6-15. Figure 6-16 shows a similar result for the negative gradient. In both the positive- and negative-gradient cases, the change in interface thick-

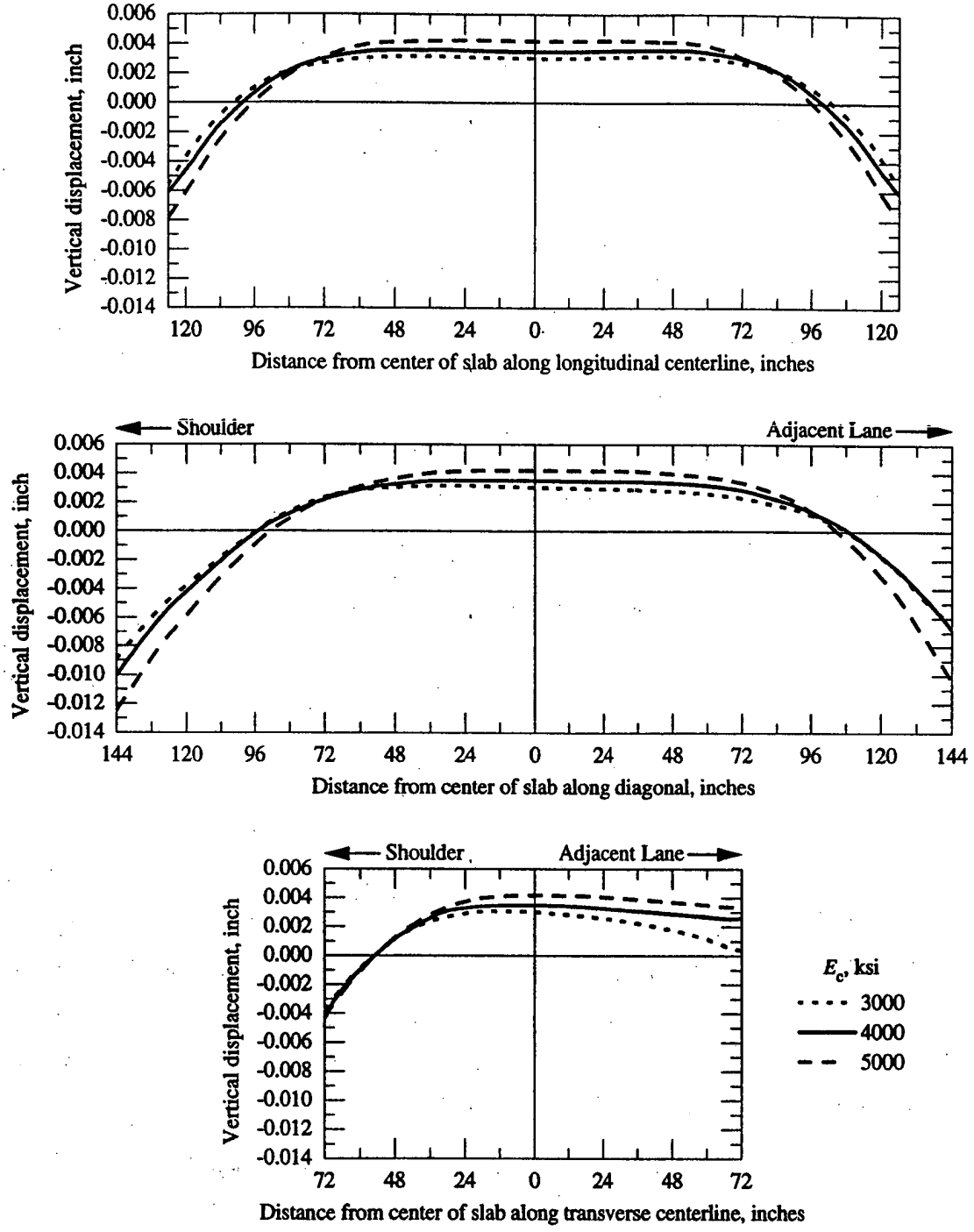

Figure 6-6. Vertical displacements of 21-foot slab for a positive tempe gradient and three elastic moduli of the concrete.

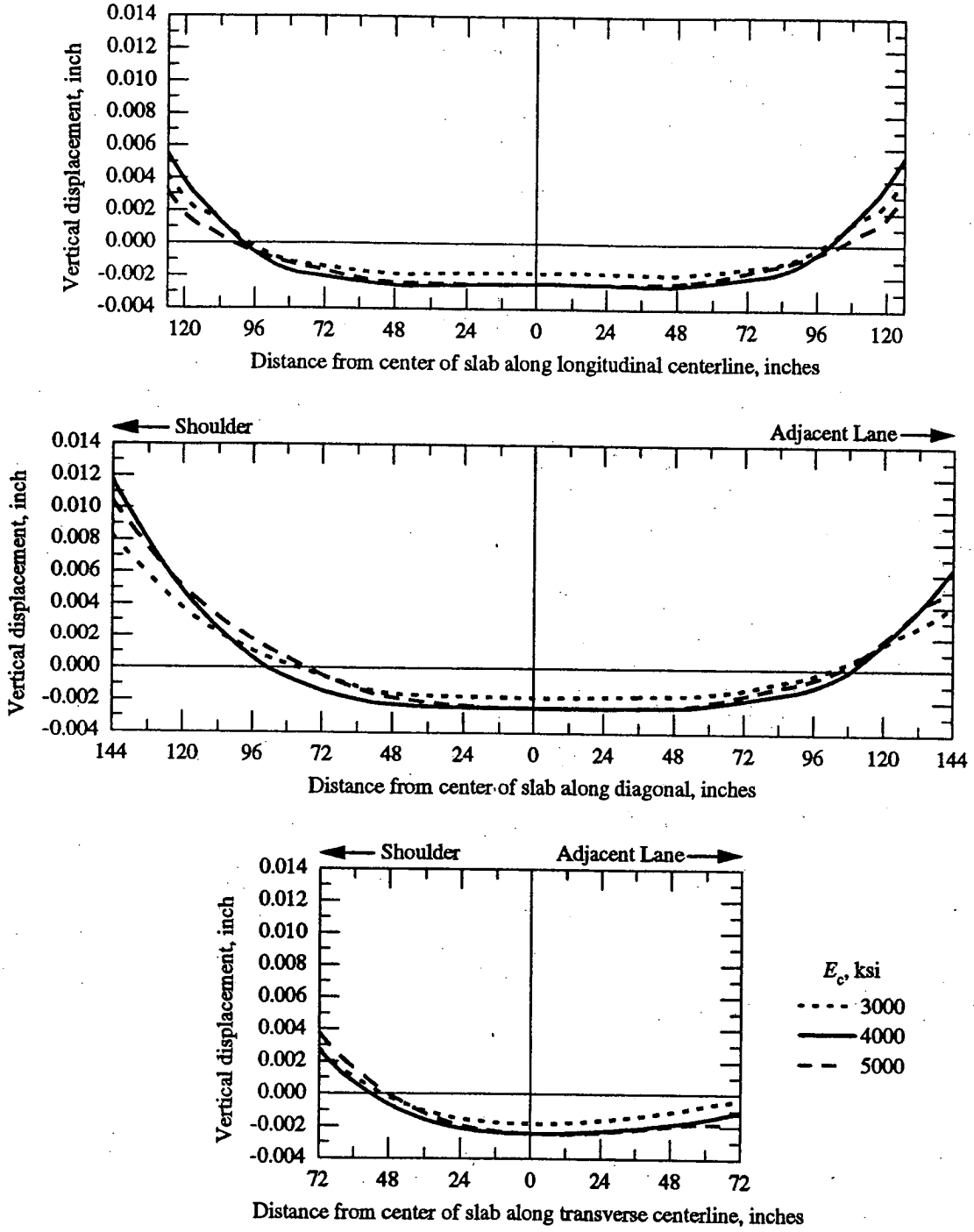

Figure 6-7. Vertical displacements of 21-foot slab for a negative temperature gradient and three elastic moduli of the concrete.

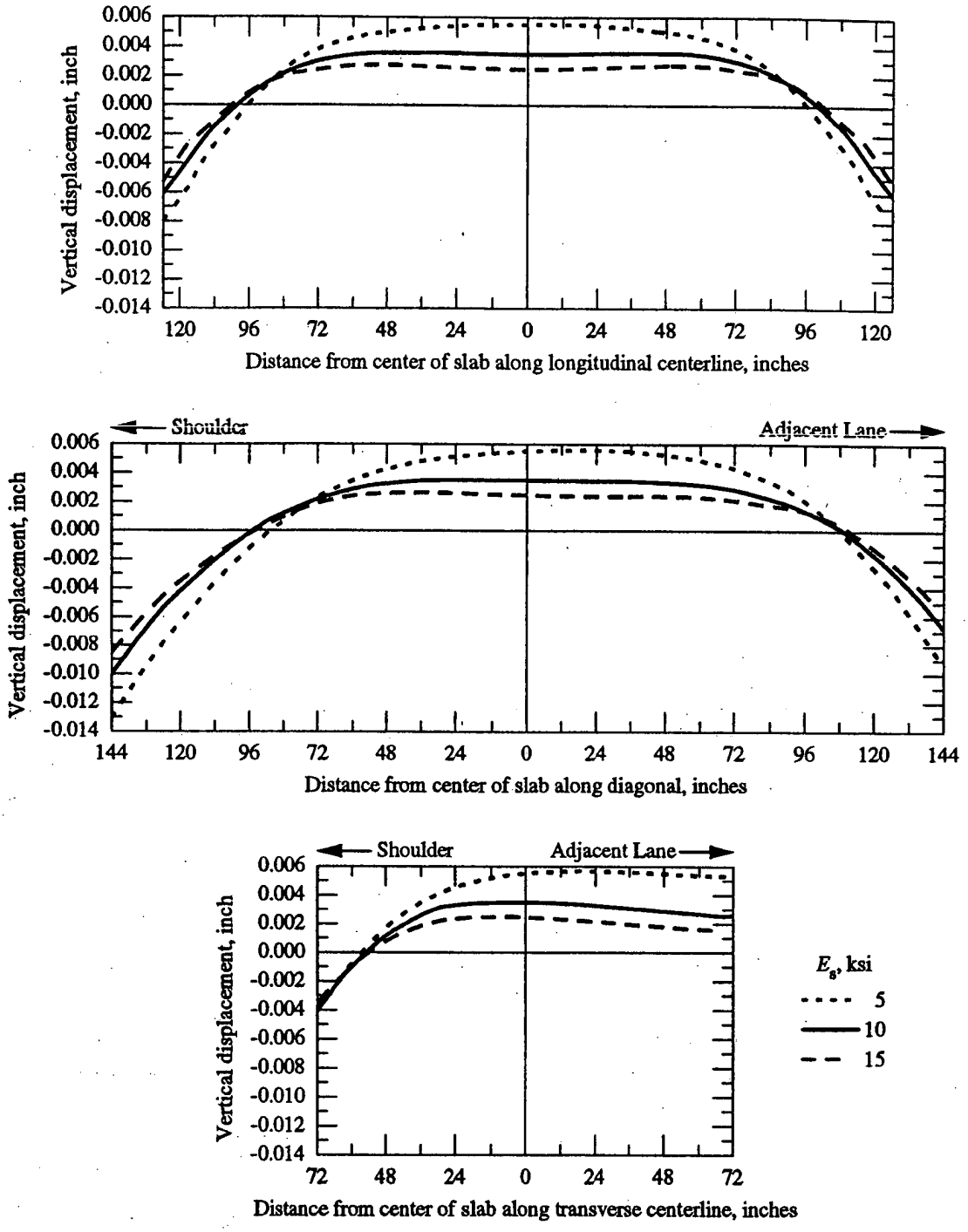

Figure 6-8. Vertical displacements of 21-foot slab for a positive temperature gradient and three elastic moduli of the subgrade.

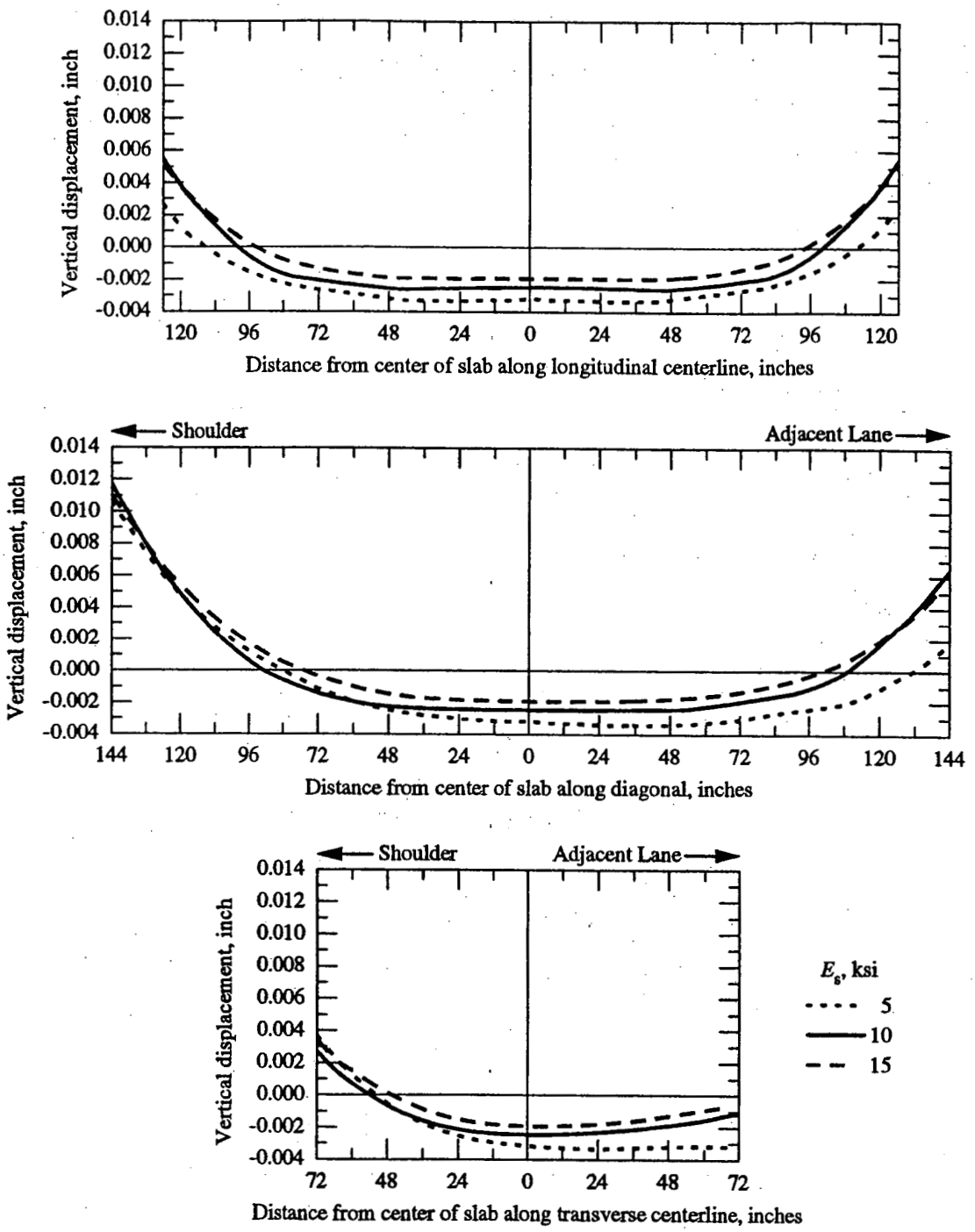

Figure 6-9. Vertical displacements of 21-foot slab for a negative temperature gradient and three elastic moduli of the subgrade.

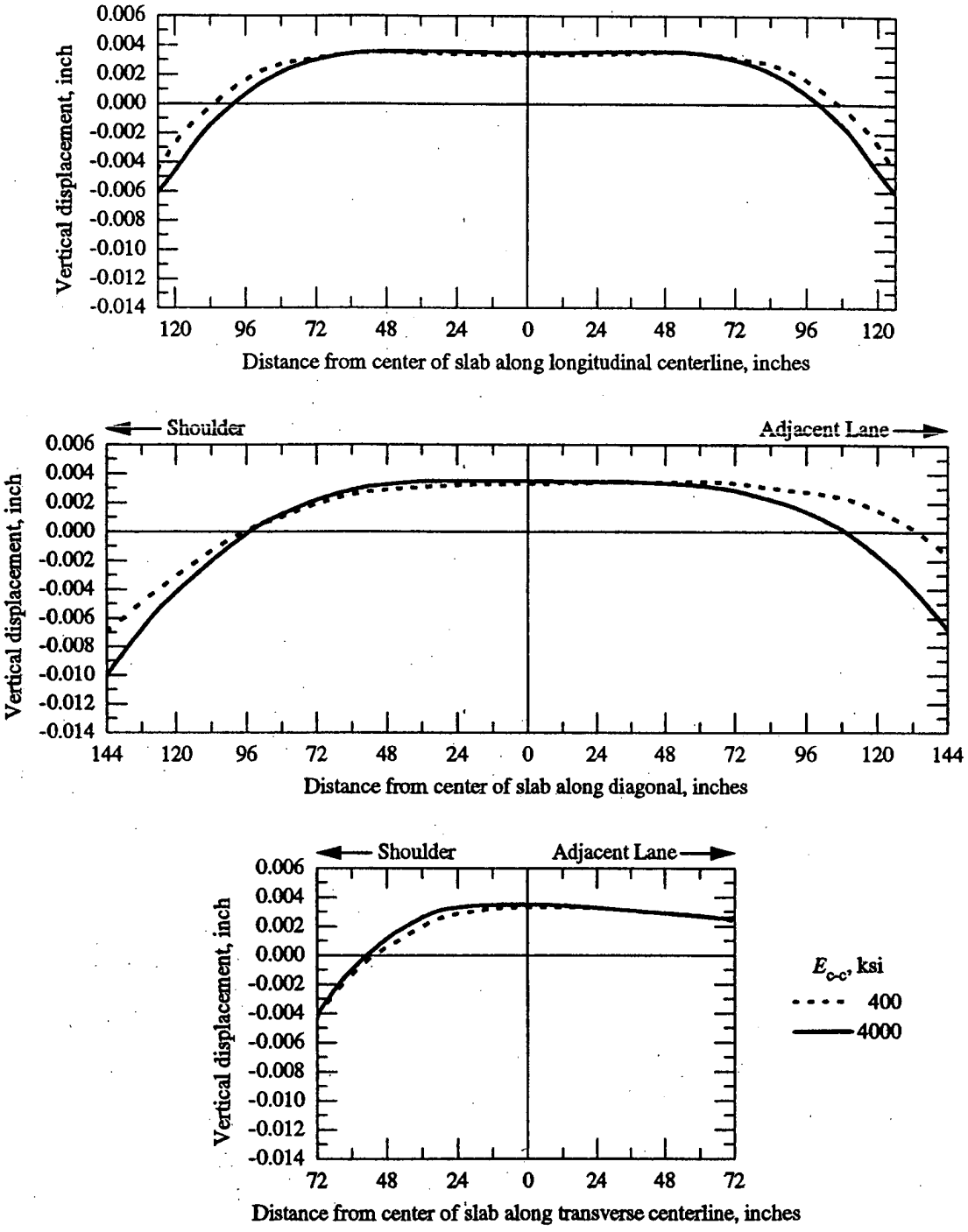

Figure 6-10. Vertical displacements of 21-foot slab for a positive temperature gradient and two elastic moduli of the concrete–concrete interface.

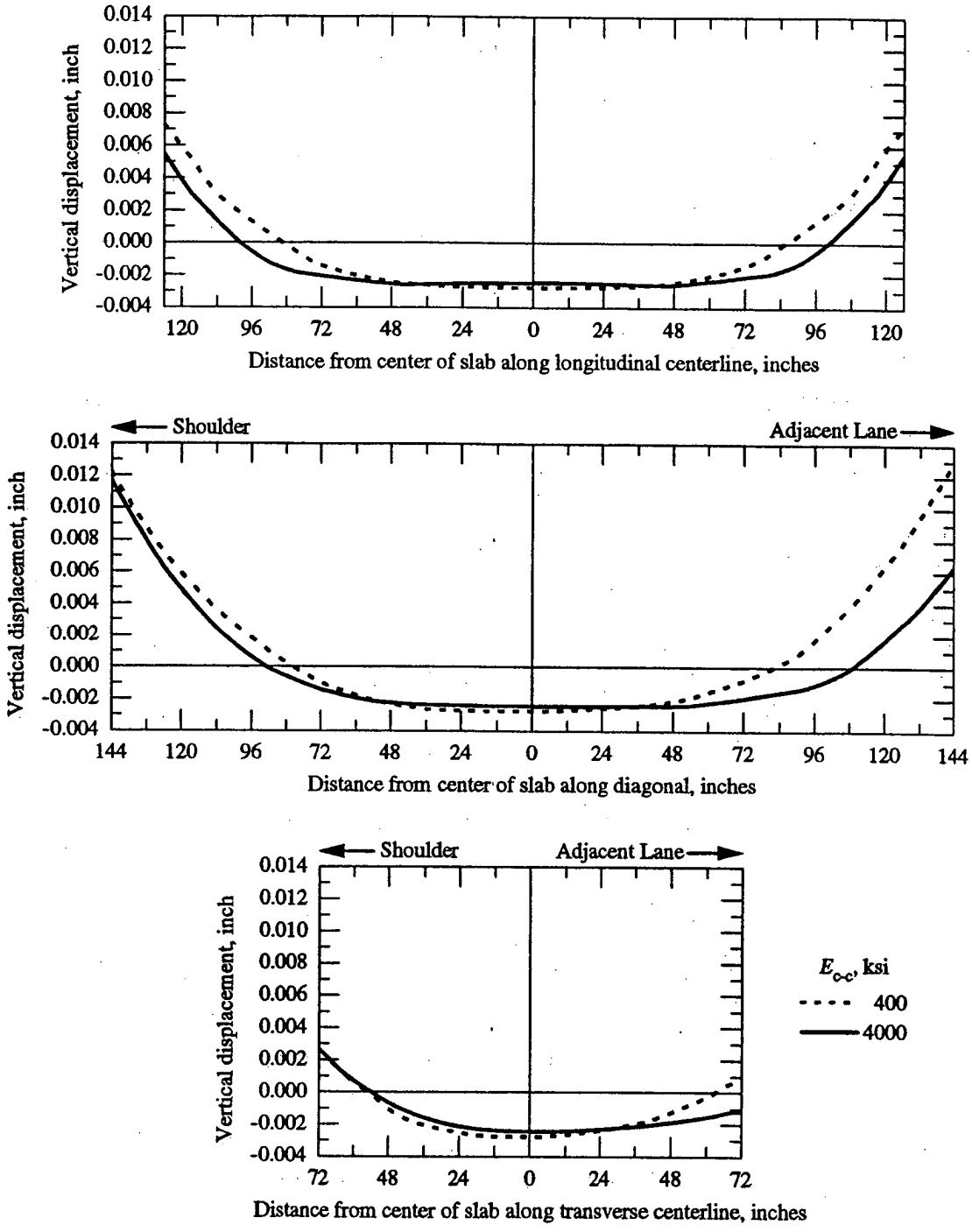

Figure 6-11. Vertical displacements of 21-foot slab for a negative temperature gradient and two elastic moduli of the concrete–concrete interface.

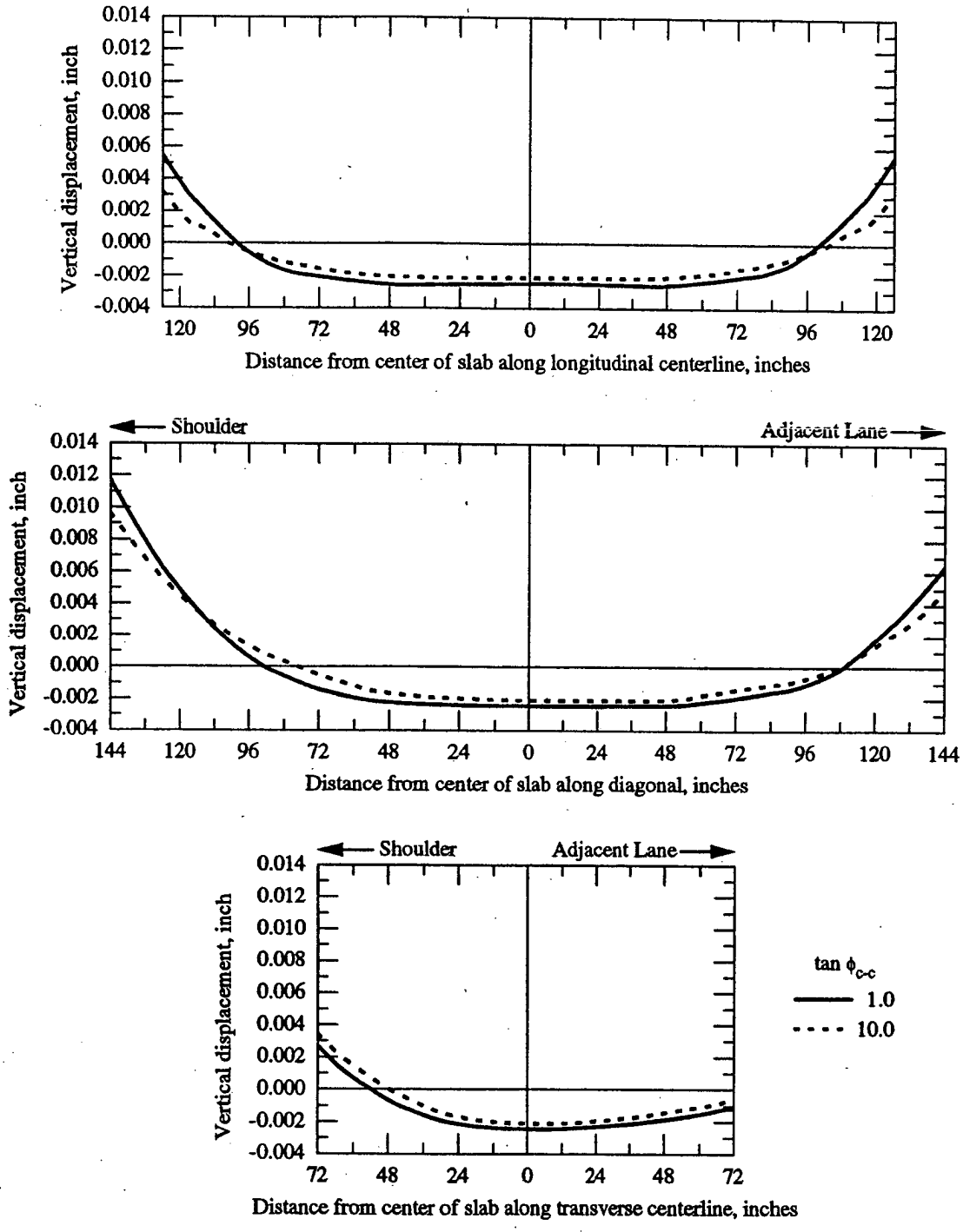

Figure 6-12. Vertical displacements of 21-foot slab for a negative temperature gradient and two friction angles of the concrete–concrete interface.

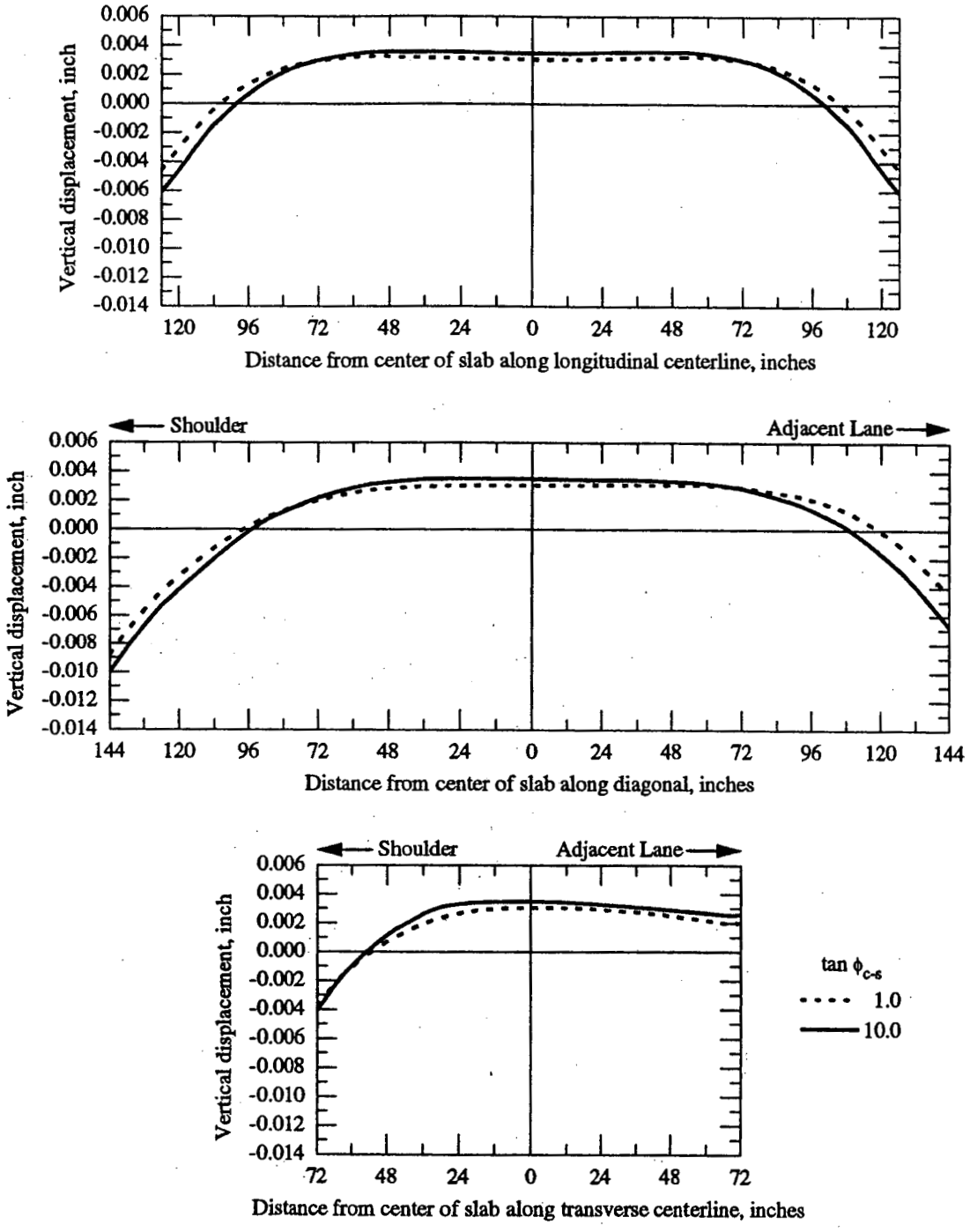

Figure 6-13. Vertical displacements of 21-foot slab for a positive temperature gradient and two friction angles of the concrete–soil interface.

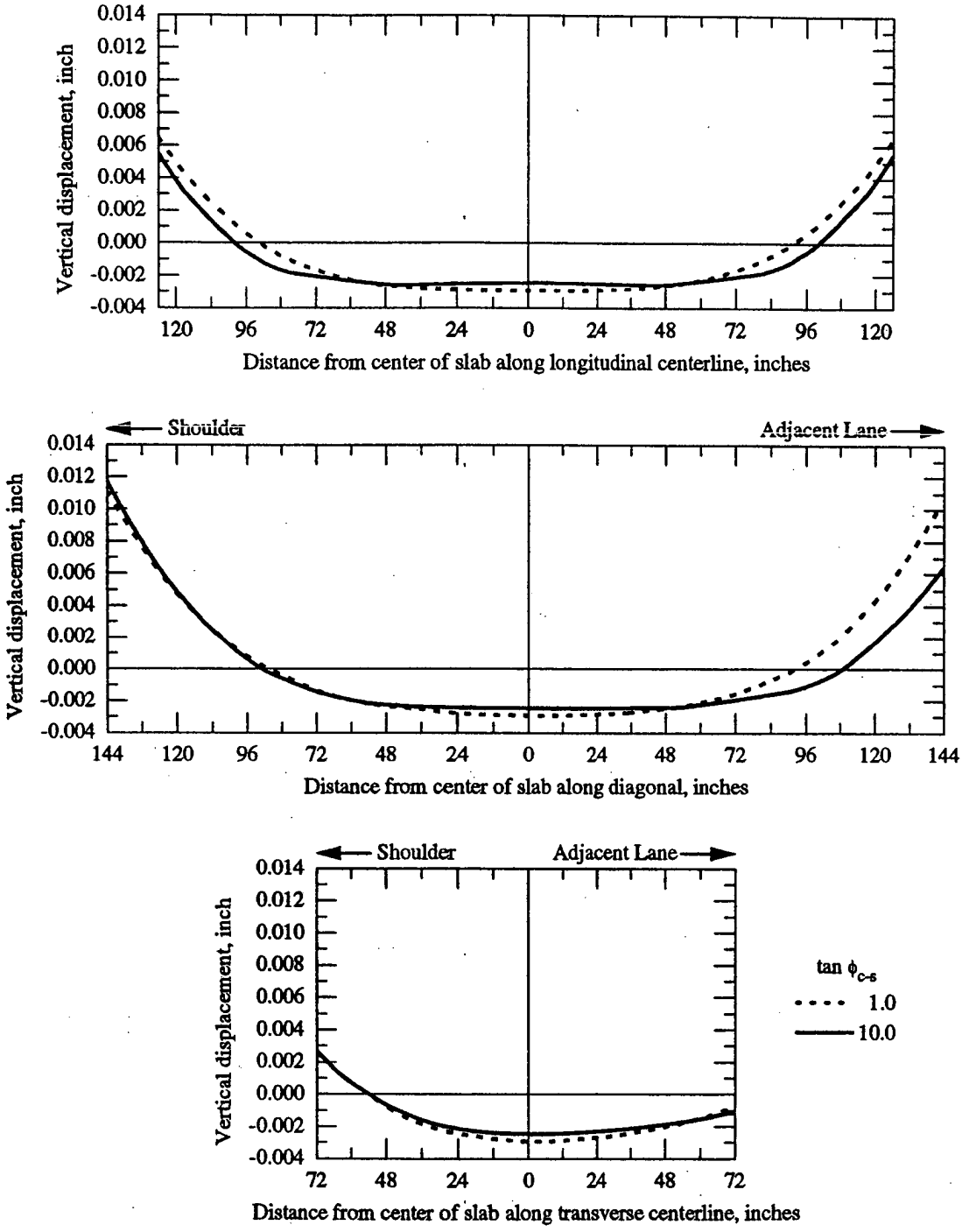

Figure 6-14. Vertical displacements of 21-foot slab for a negative temperature gradient and two friction angles of the concrete–soil interface.

ness from one inch to two inches produced a much greater change in the displacements than was caused by the change from the half-inch to the one-inch interface thickness.

6.2.5 Dowels and Ties. Different dowel diameters made almost no difference in the displacements. The tie diameter, on the other hand, had a significant influence on the negative-gradient displacements, as Figure 6-17 shows.

6.2.6 Shoulder. In general, the addition of a tied shoulder to the mesh reduced the magnitude of the displacements along the shoulder edge of the slab and increased their magnitude along the opposite edge. Figure 6-18 shows the results for the positive temperature gradient, and Figure 6-19 shows the results for the negative gradient.

6.2.7 Average Temperature Change. Figure 6-20 shows the displacements for five different average temperature changes with the same positive temperature gradient. Figure 6-21 shows the corresponding curves for the negative temperature gradient. The curves for the two positive temperature changes are similar in both figures, as are the curves for the two negative temperature changes. The major change in the displacements occurs in the transition from positive to negative average temperatures. This can be understood by recalling that the concrete–concrete interface elements lose their stiffness in tension. Therefore the joints have very small stiffness when the average temperature change is negative. The opposite is true when the average temperature change is positive. The joints are in compression, and the edges of the slabs are not as free to move.

6.3 Experimental Data

Figure 6-22 shows vertical displacements along the centerline and along the end joint as well as longitudinal stresses along the centerline for all of the positive-gradient finite-element problems corresponding to all of the material properties given in Table 6-1. The graphs also show some experimental data. The graphs for the negative temperature

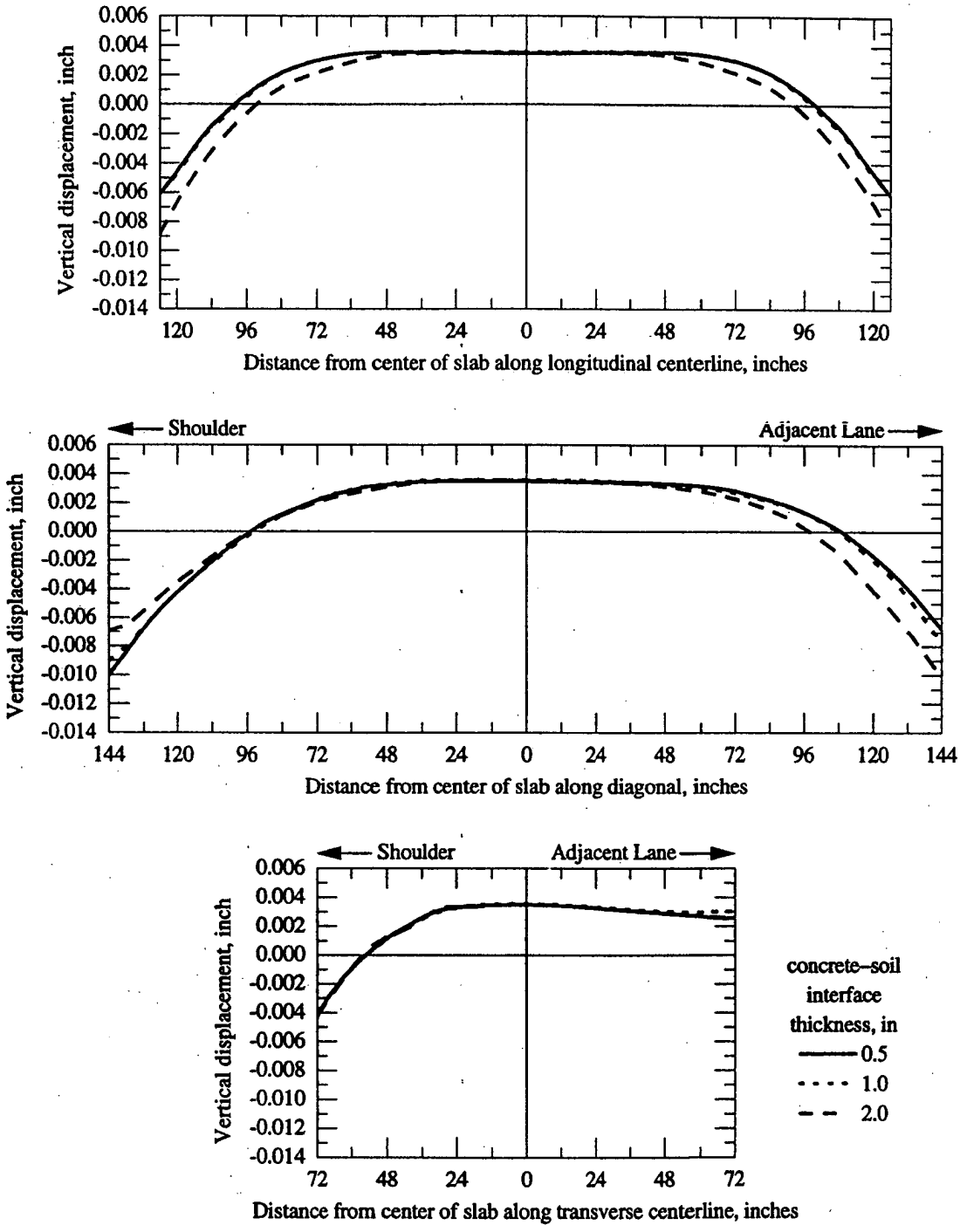

Figure 6-15. Vertical displacements of 21-foot slab for a positive temperature gradient and three thicknesses of the concrete–soil interface.

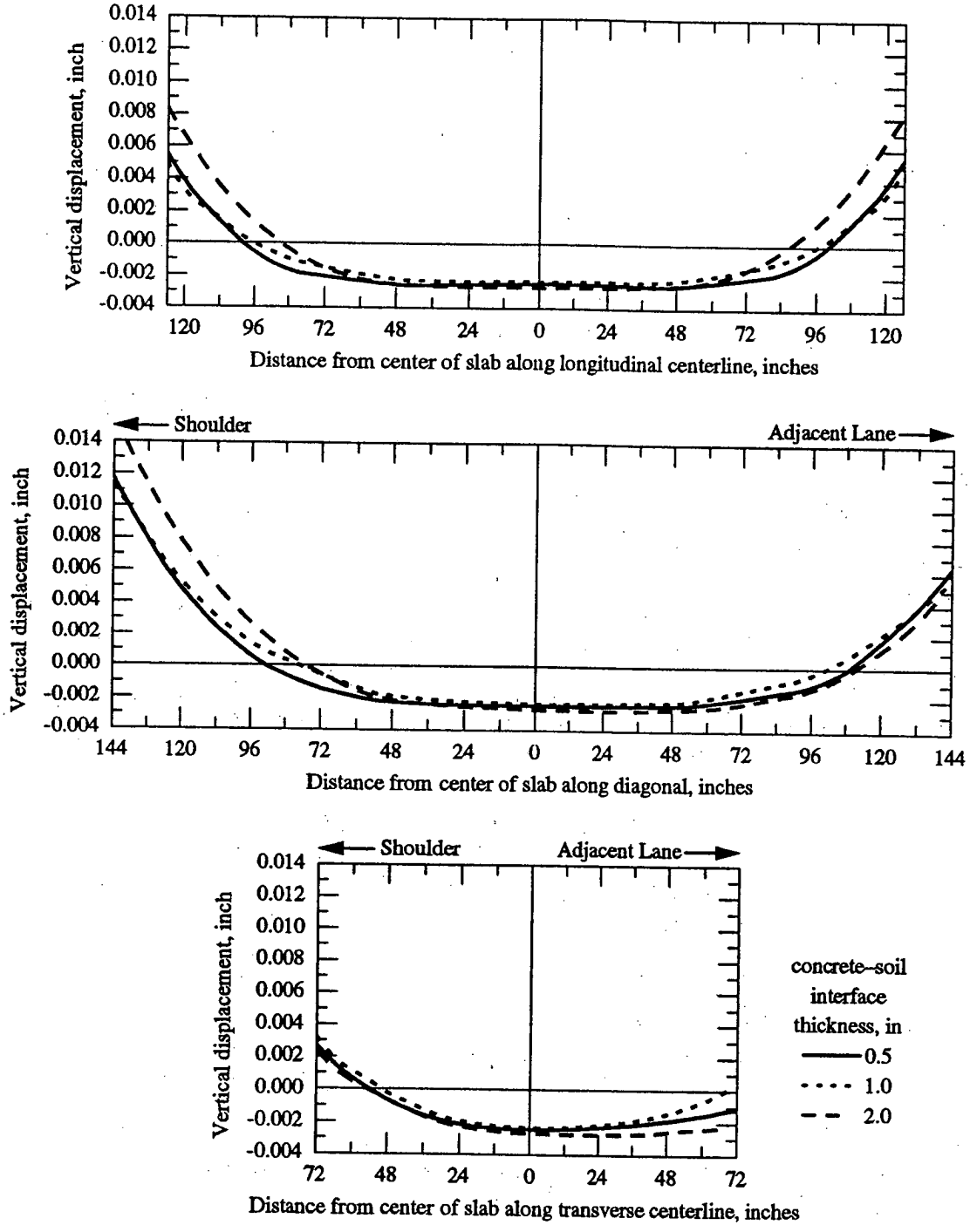

Figure 6-16. Vertical displacements of 21-foot slab for a negative temperature gradient and three thicknesses of the concrete–soil interface.

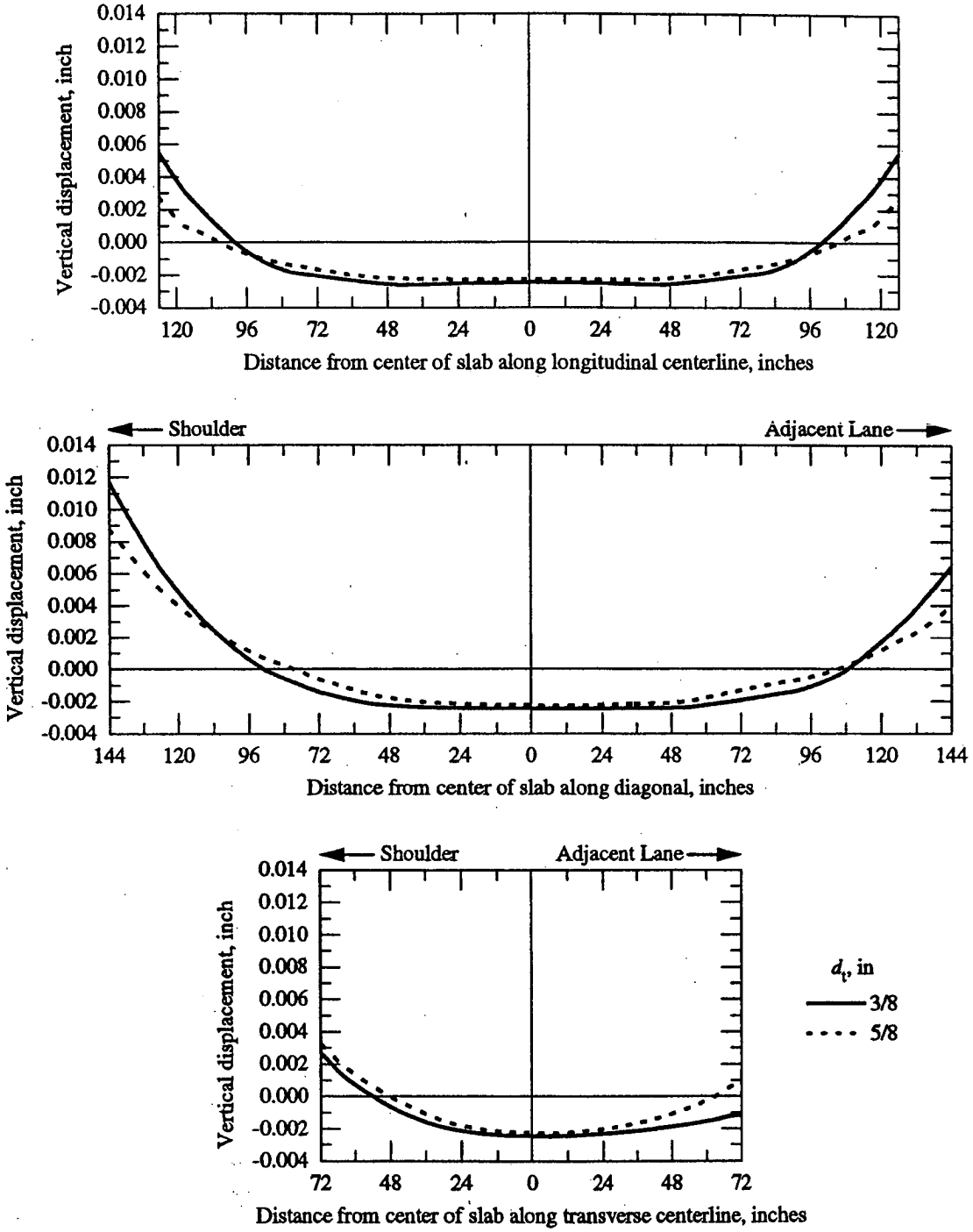

Figure 6-17. Vertical displacements of 21-foot slab for a negative temperature gradient and two tie diameters.

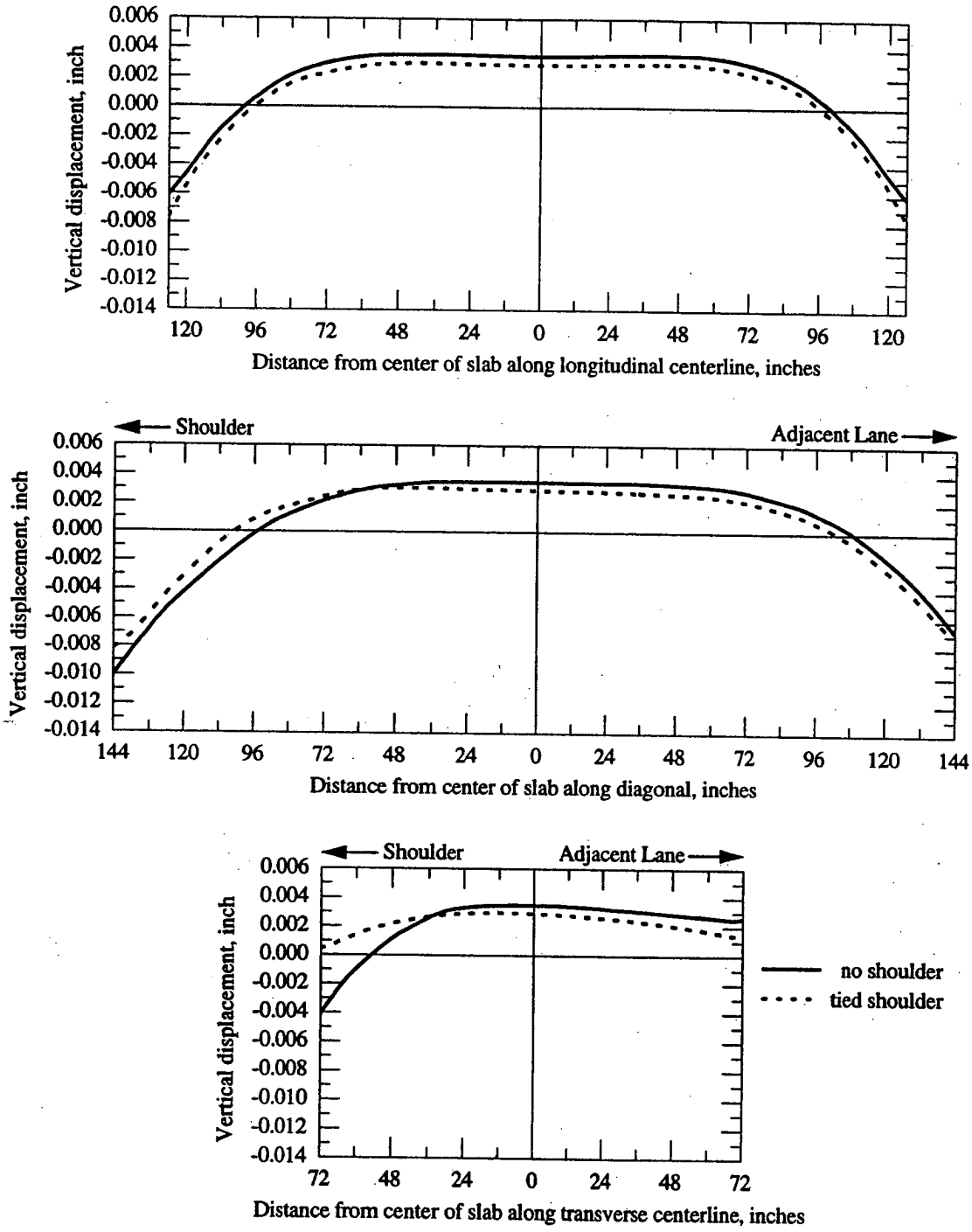

Figure 6-18. Vertical displacements of 21-foot slab for a positive temperature gradient and a tied shoulder.

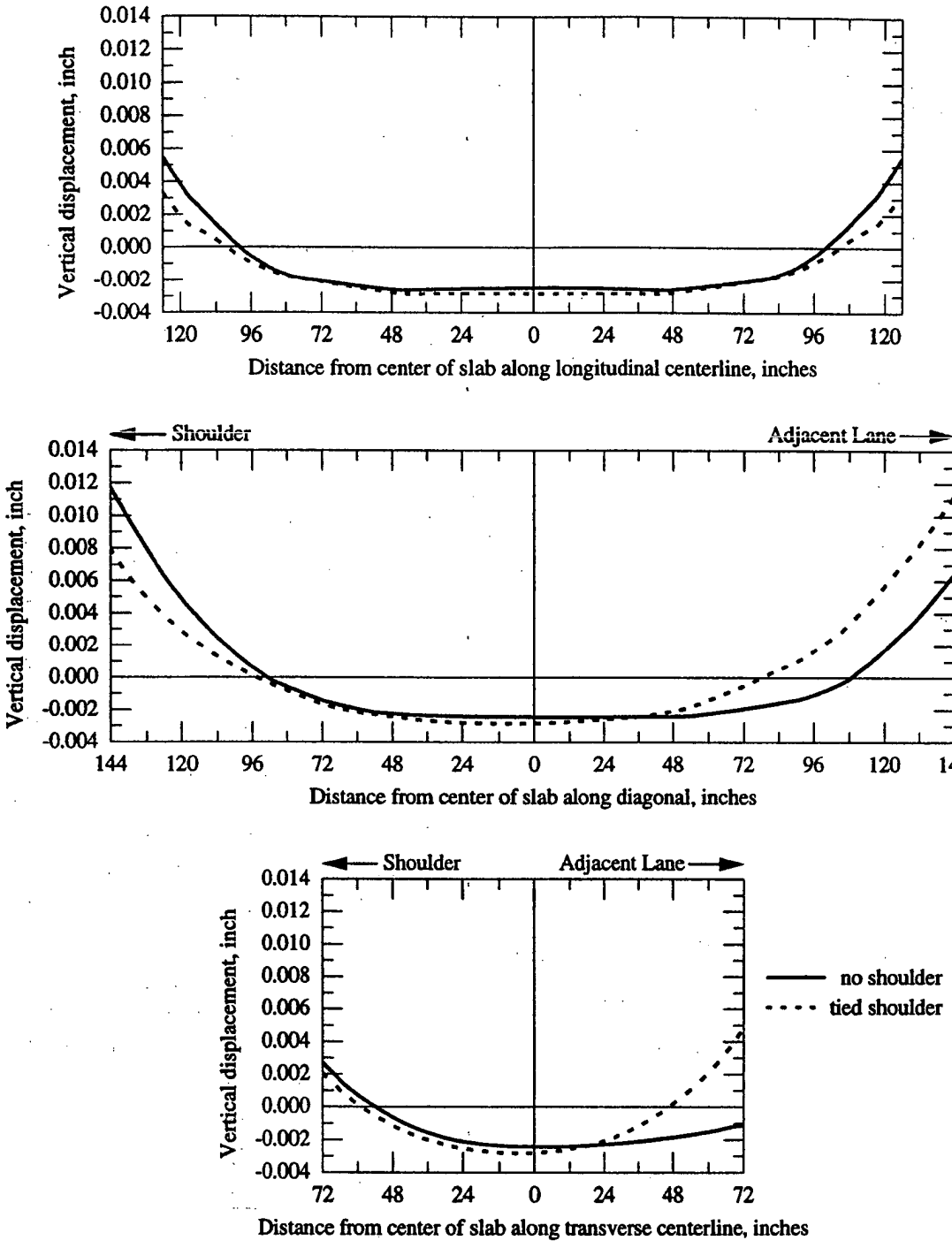

Figure 6-19. Vertical displacements of 21-foot slab for a negative temperature gradient and a tied shoulder.

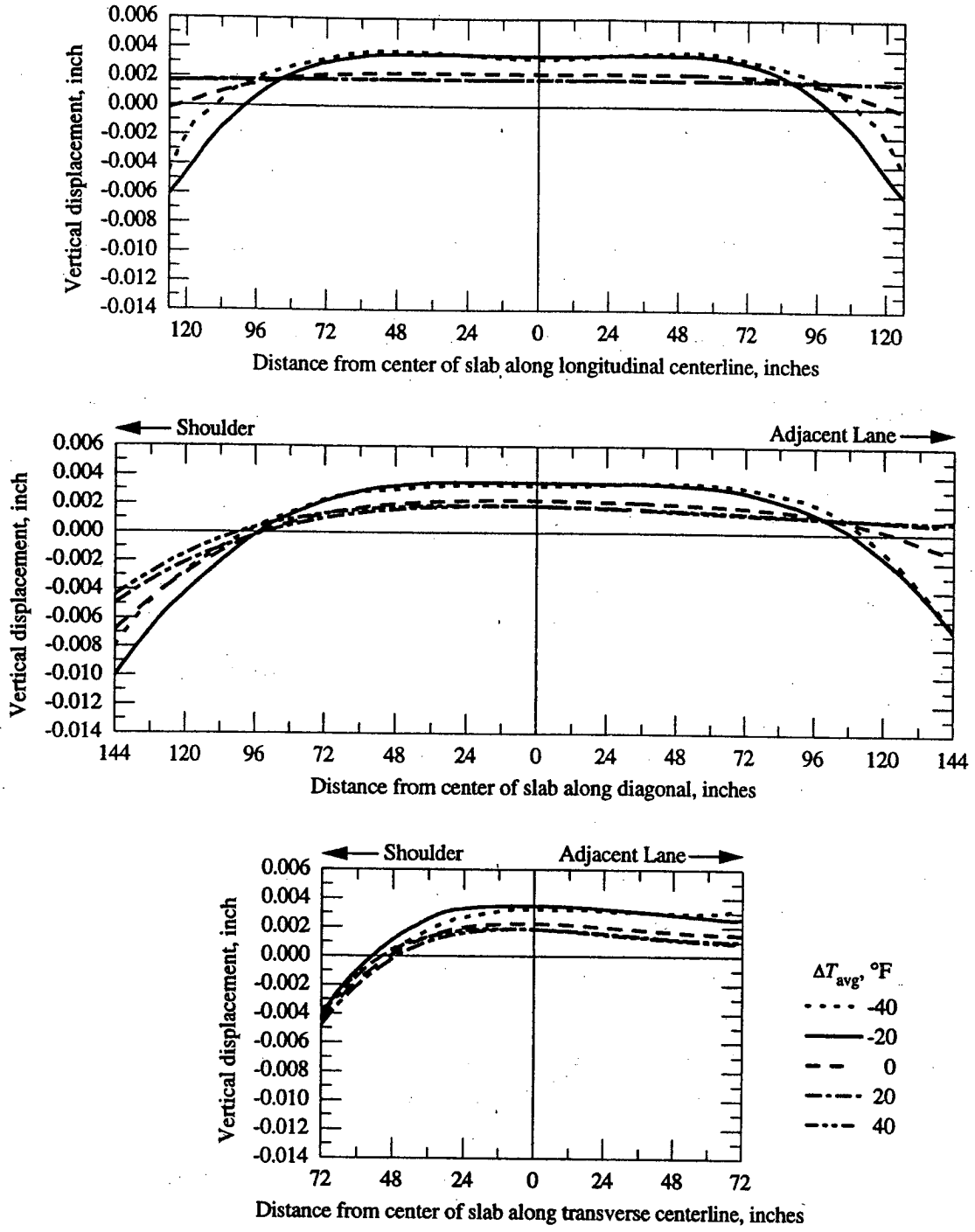

Figure 6-20. Vertical displacements of 21-foot slab for a positive temperature gradient and five average temperature changes.

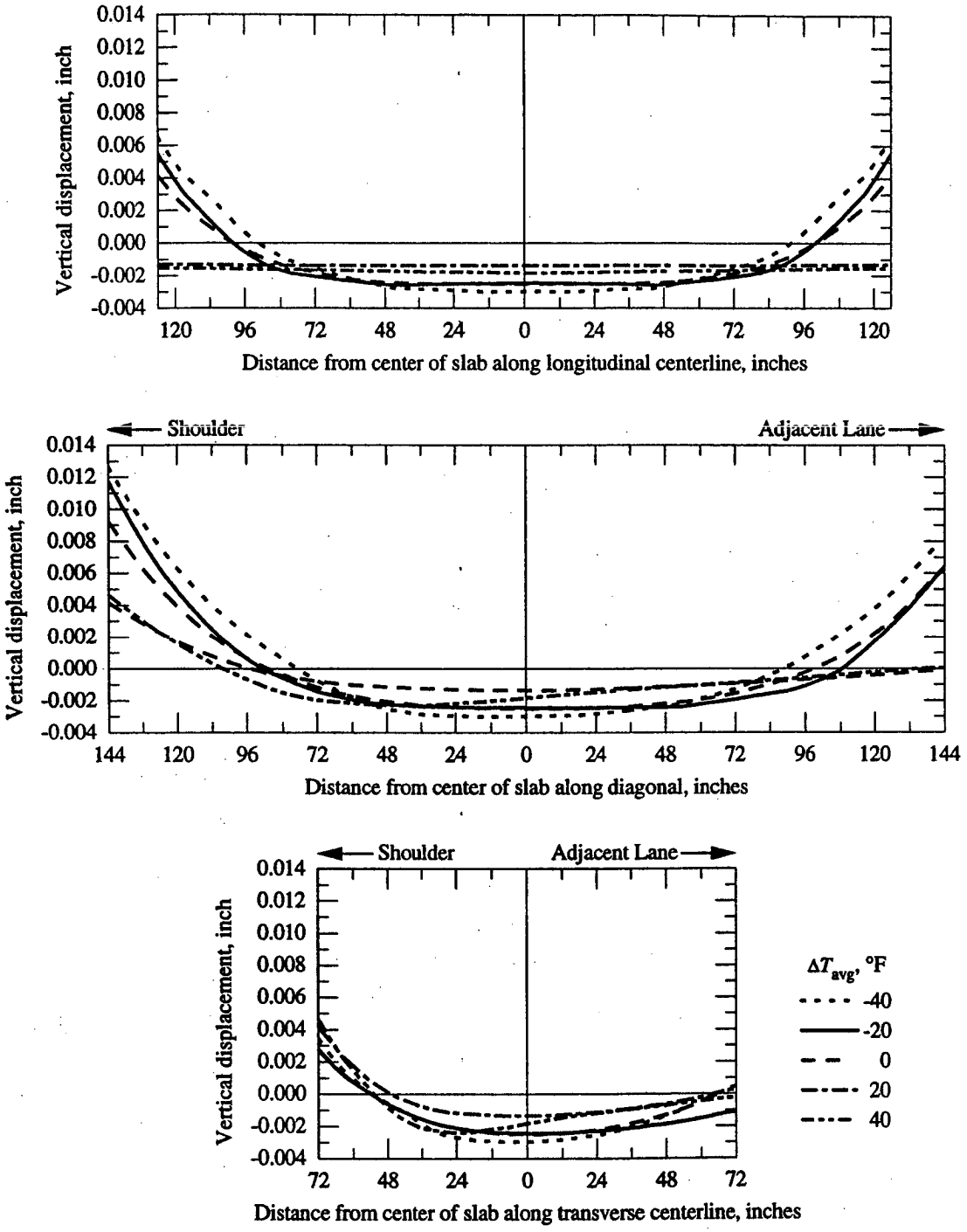

Figure 6-21. Vertical displacements of 21-foot slab for a negative temperature gradient and five average temperature changes.

gradient are in Figure 6-23. In both cases the displacements agree fairly well, but the stresses do not match as closely. Several factors probably contribute to the discrepancy, possibly including an uncertainty in the depth of the strain gages, nonuniform support under the slab, complex behavior of the concrete–concrete interfaces, and, of course, non-linear material behavior.

6.4 Axle Loads

Problems were run with axle loads at the end joint and at the centerline. In each problem, the axle load was 15 tons and was distributed over two 216-square-inch areas centered at 36 and 120 inches from the shoulder. Because of the symmetry of the finite-element mesh, these problems actually represent a situation in which the same load is present on the adjacent lane and the loads are repeated at the center of each slab or at each end joint. Figure 6-24 shows the vertical displacements of a slab loaded at its center with and without a positive temperature gradient. The stresses along the transverse centerline are shown in Figure 6-25. The displacements of a slab loaded at the joint are shown in Figure 6-26, and the stresses are in Figure 6-27. These problems were run with a negative temperature gradient.

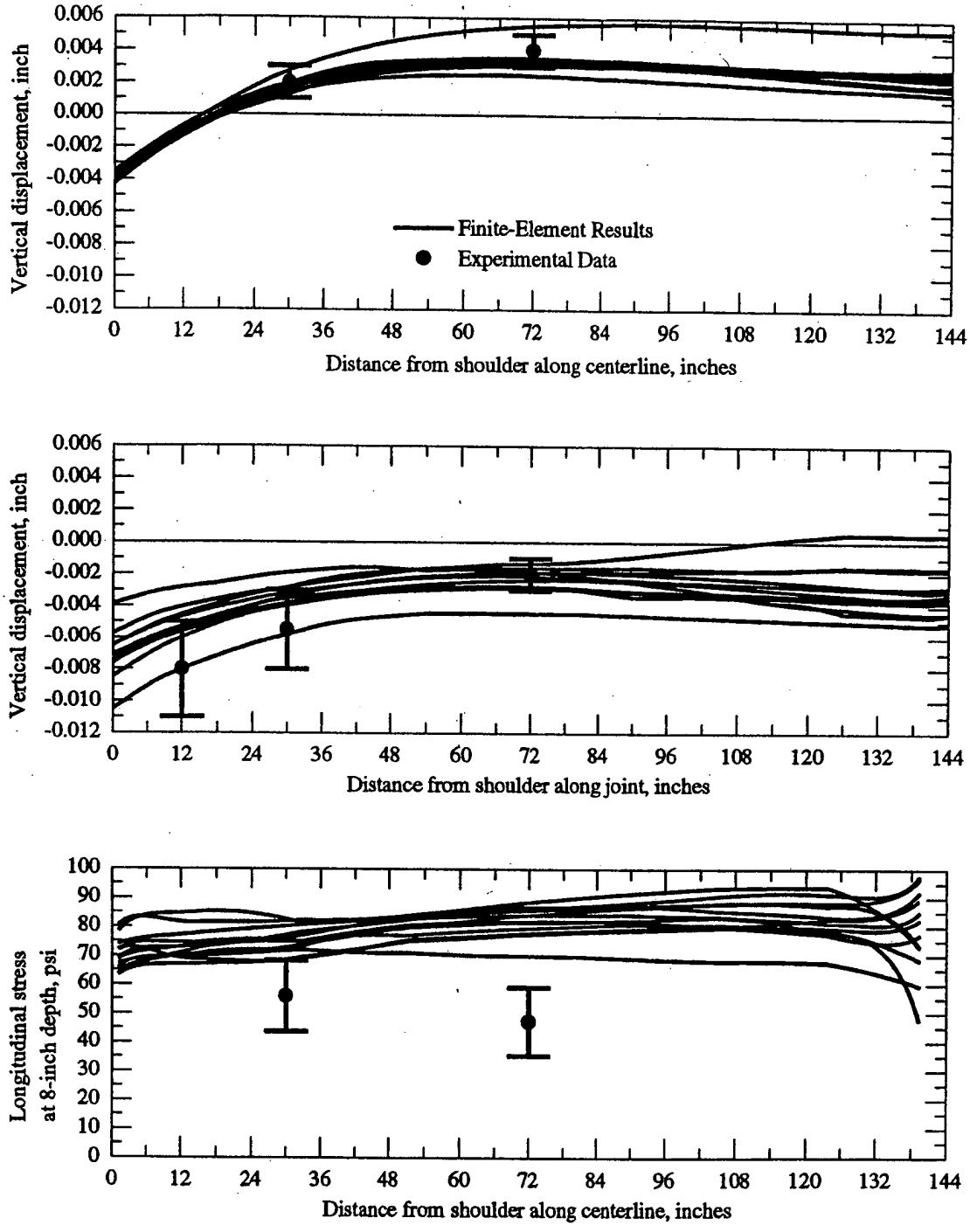

Figure 6-22. Comparison of displacements and stresses from finite-element problems with experimental data for positive temperature gradient.

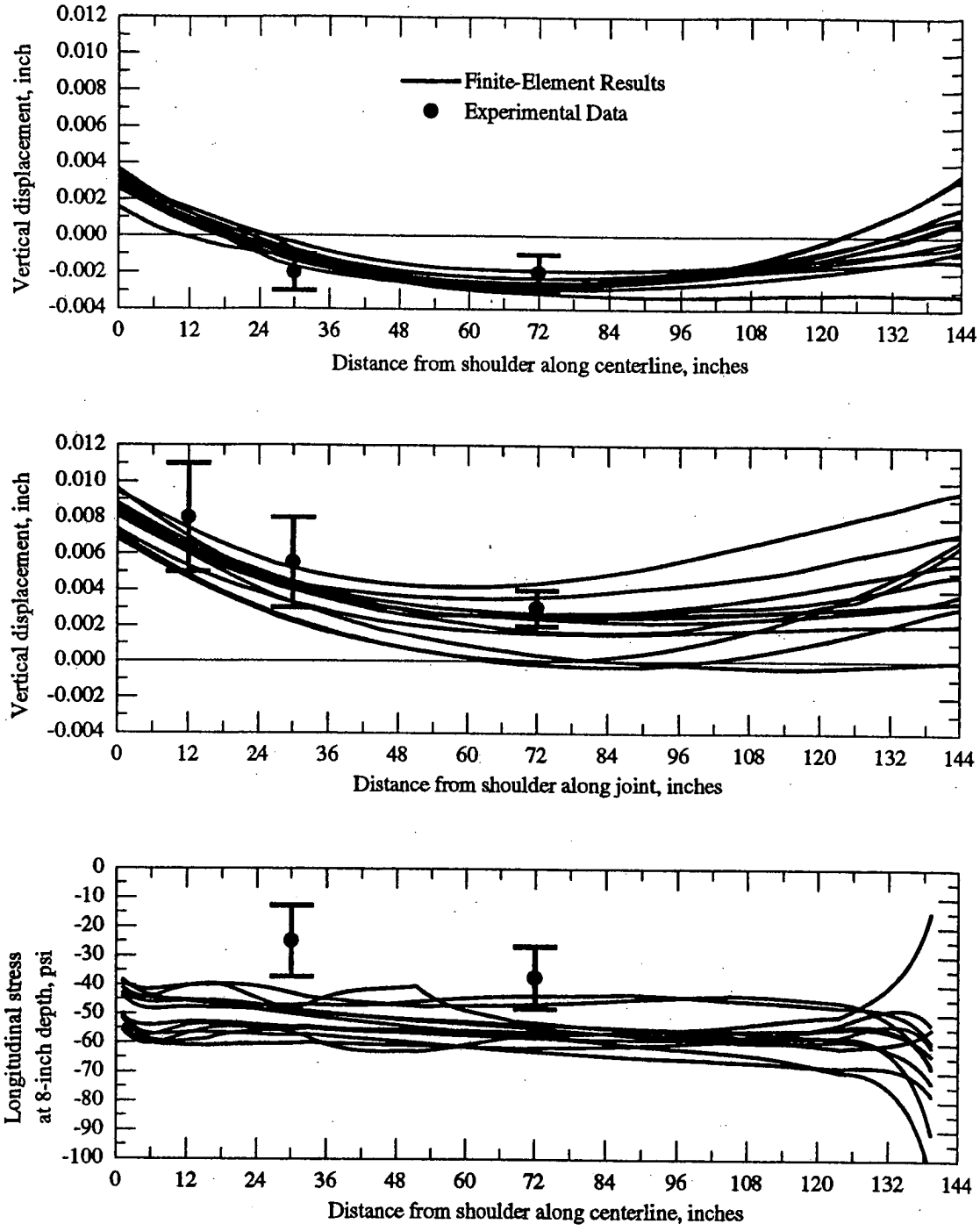

Figure 6-23. Comparison of displacements and stresses from finite-element problems with experimental data for negative temperature gradient.

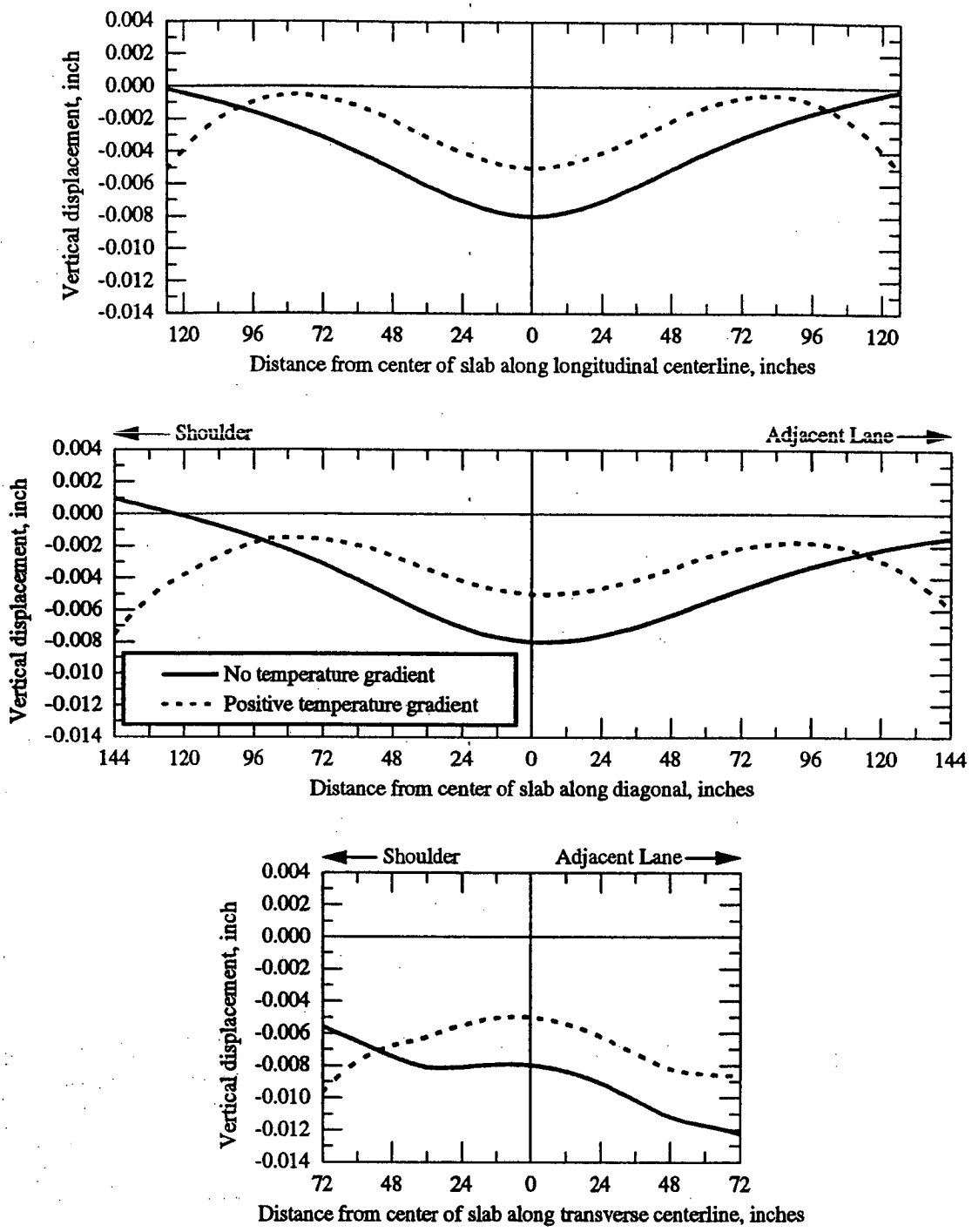

Figure 6-24. Vertical displacements of 21-foot slab with 15-ton axle load at center.

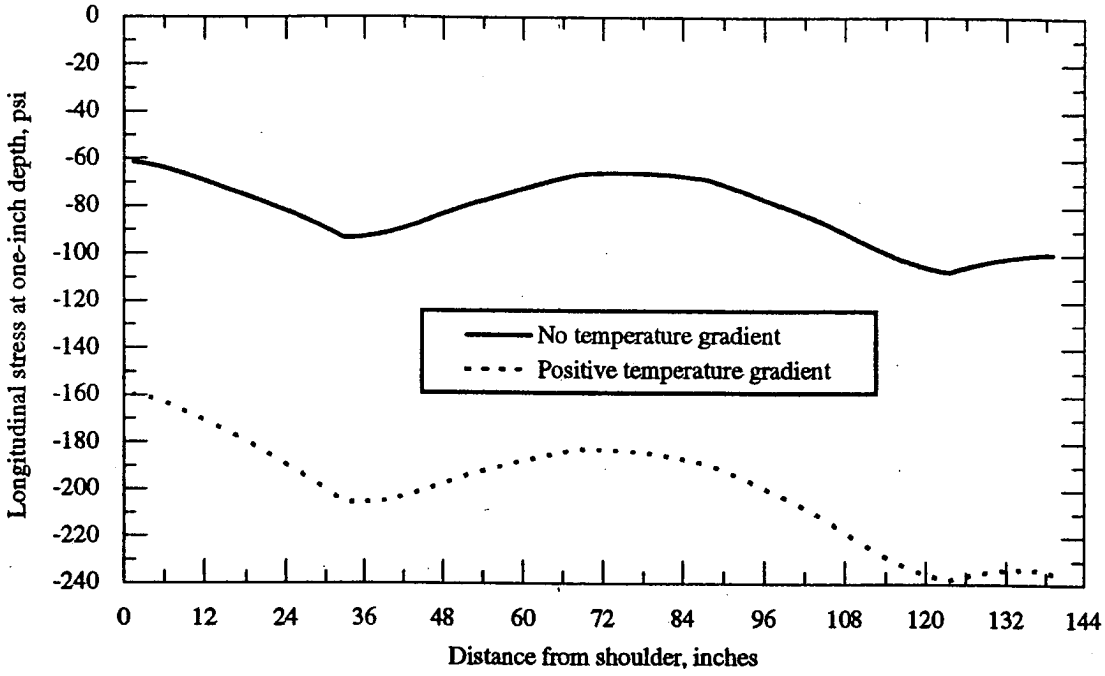

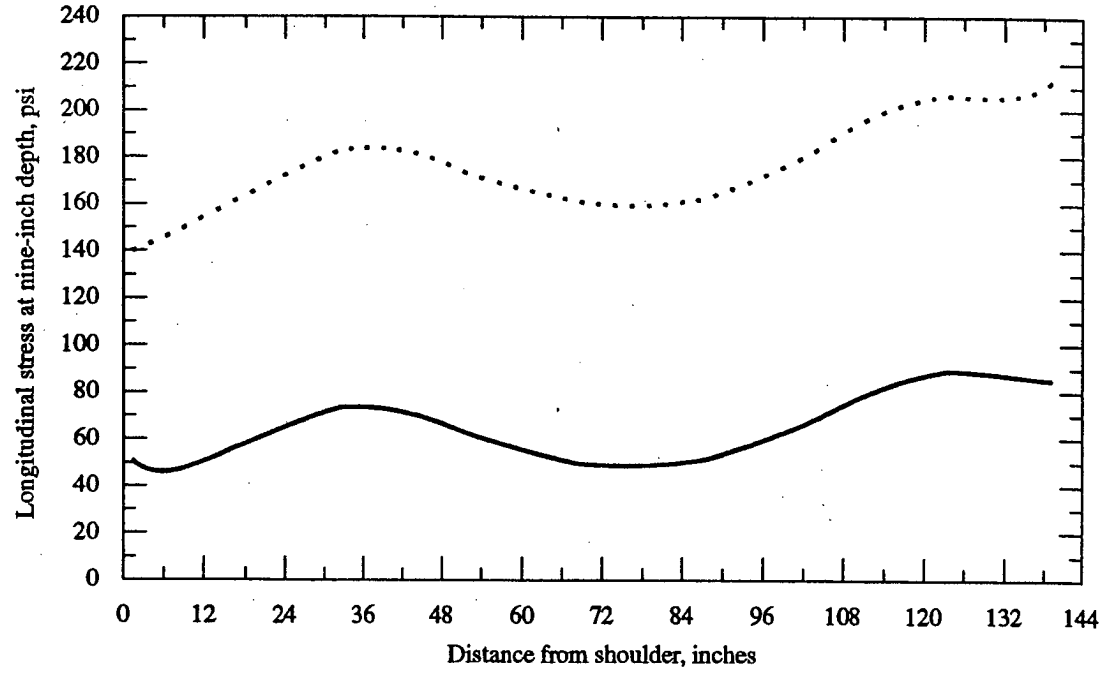

Figure 6-25. Longitudinal stresses along transverse centerline of 21-foot slab with 15-ton axle load at center.

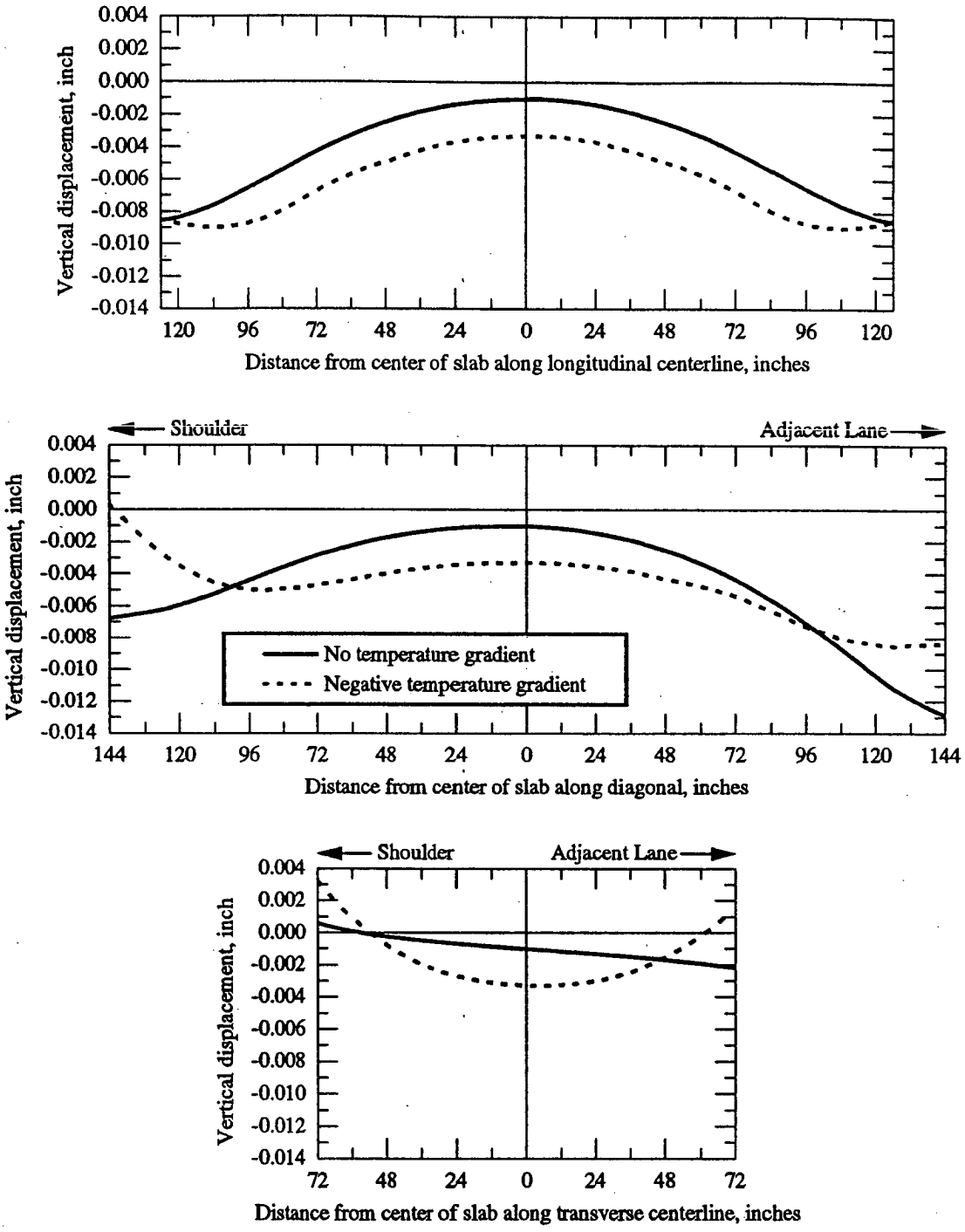

Figure 6-26. Vertical displacements of 21-foot slab with 15-ton axle load at joint.

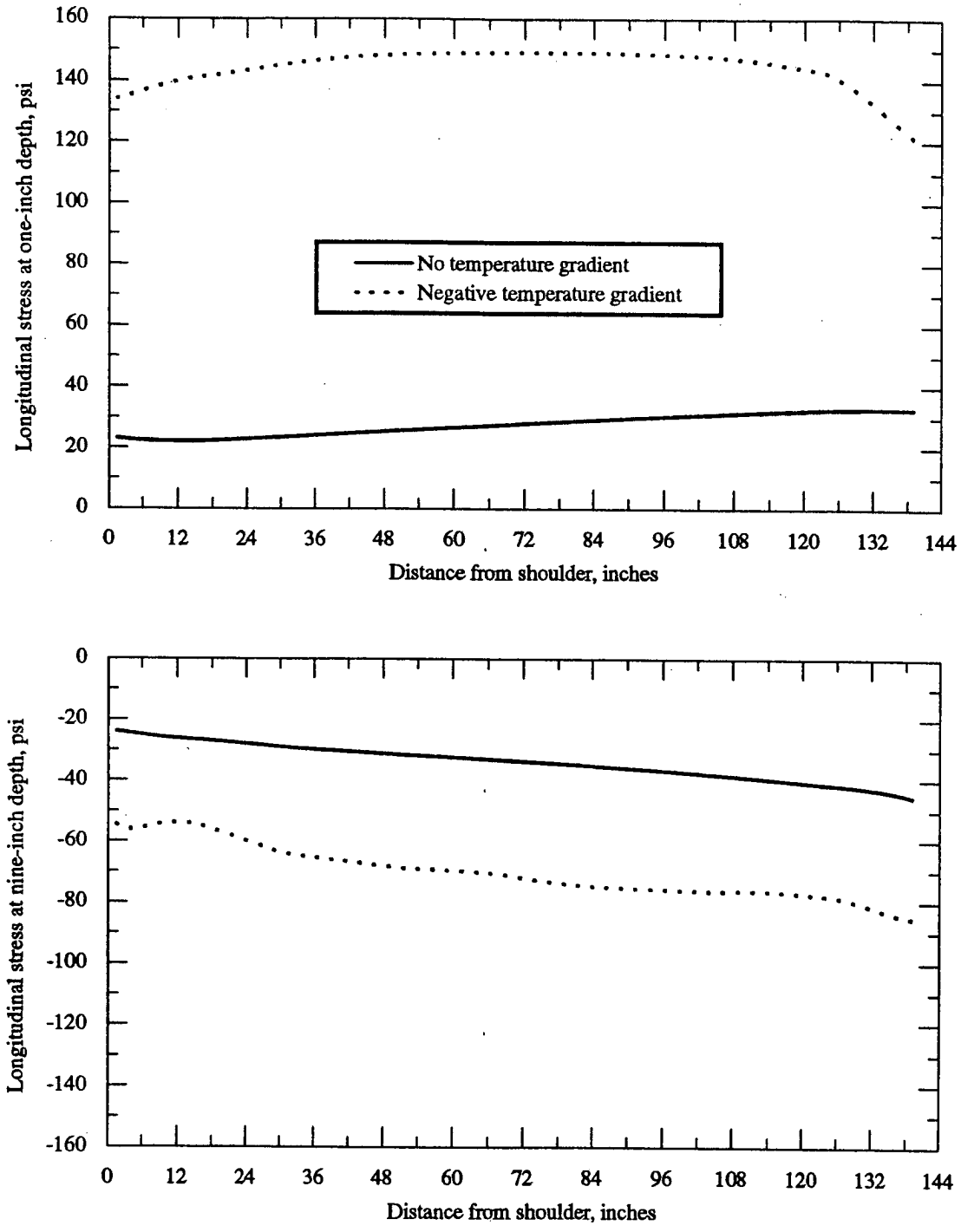

Figure 6-27. Longitudinal stresses along transverse centerline of 21-foot slab with 15-ton axle load at joint.

7
Conclusion

7.1 S ary

A three-dimensional finite-element program has been described which was developed to model rigid pavement under static loads and thermal gradients. Features of the program include the ability to model dowel bars, pavement joints, and concrete–soil interfaces. The program which has been described has proved to be capable of predicting accurately the displacements of a rigid pavement slab under a thermal gradient loading. Predicted stresses have differed from experimental data by a greater margin, but they have been in at least reasonable agreement. Better results probably could be obtained by extending the program to model nonlinear concrete behavior, pavement cracking, and steel reinforcement.

7.2 Recommendations for Future Investigation

Below are listed several improvements and additions which could be made to the program. They are listed in estimated order of effort (both human and computational) required for implementation.

1. Add a nonlinear elastic concrete model
2. Add a concrete reinforcement model.

3. Add a nonlinear soil model with properties dependent on moisture.
4. Add an inelastic concrete cracking model.
5. Implement a viscoelastic model for asphalt pavement.
6. Modify the program to model dynamic response to impulse loads, and compare data from a falling-weight deflectometer test.
7. Add the ability to model moving axle loads.

The last few of these would require much greater computational power than was available for this study.

Some possibilities for further study which would require little or no modification to the program are the following:

1. Investigate the region of the slab near the joint with a very fine mesh. The concrete–dowel bonding could be simulated with thin interface elements, and the dowels could be represented by the same twenty-node hexahedral elements presently used for concrete and soil.
2. Attempt to make an experimental determination of the residual stresses in a slab. The residual stresses could be input to the program as initial stresses. If the residual stresses were significant, the result would likely be improved agreement between the predicted and experimental stresses and displacements.

References

1. E. Hinton and D. R. J. Owen, *Finite Element Programming*, Academic Press, London, 1977, 68–78.
2. W. Weaver Jr. and P. R. Johnston, *Finite Elements for Structural Analysis*, Prentice-Hall, Englewood Cliffs, New Jersey, 1984, 159–161.
3. O. C. Zienkiewicz and R. L. Taylor, *The Finite Element Method*, 4th ed., vol. 1, McGraw-Hill, London, 1989, 133.